Michael Sarnthein et al.

Dear Editor, Dear André Paul,

With thanks we obtained your helpful recent comments and tried to include them with care into our manuscript. A detailed response to the points you raised you will find below: They are marked by arrows "in between your lines".

We now hope that the present version of our manuscript may be satisfactory to be accepted for publication in C.P.

Yours sincerely,

Michael Sarnthein and coauthors.

,,

Editor Decision: Publish subject to minor revisions (review by editor) (30 Jul 2020) by C.P. editor André Paul: Comments to the Author:

Dear Authors,

Thank you for submitting a revised version of your manuscript. Unfortunately, I think that it is not quite the final version, because it differs in a few points from your response to the points (1) and (2) that I had raised before:

(1) Unpublished data and manuscripts "in prep."

I accept your decision to put your manuscript on hold until the two manuscripts by Ausin et al. and of Küssner et al.

become publicly available (which probably means until they are accepted for publication) and the embargo on the related data sets on PANGAEA will be lifted.

--> Embargo on the crucial data sets of Ausin et al. and Küssner et al. on PANGAEA will be lifted by September.

As one of our reviewers suggested, readers should not necessarily believe what is written but rather look at primary data themselves. For this reason, we shall keep you as editor informed, when the data are publicly available and we shall ask you for a lift of the "on hold" status of our paper as soon as the embargo of the data at PANGAEA will be released.

In the revised version of the manuscript, the following citations would need to be corrected: --> our recent pertinent changes are marked RED

Line 264: Ausin et al., 2020 subm.

--> the present raw draft of this manuscript will be ready for submission to P&P after the vacations in September.

Line 637: Ausin et al. (in prep.)

--> now converted to '2020 subm.'

Line 171, 263, 476, 481, 503, 591-592, 636, 669, 847, 1338: Küssner et al., 2020 subm.
--> the manuscript is now under review at P & P.
A QUESTION: Would you as editor prefer a change of all citations to "Küssner et al., 2020, under review"?

In addition, the manuscripts by Ausin et al. would need to be added to the list of references, while the reference to Küssner et al. in lines 973-975 would need to be completed.
--> Proper refs to Ausin and Küssner are now included!

(2) Personal communication ("pers. com")

In contrast to your response, I cannot find the reference to the paper by Bronk Ramsey "now published under 2020"".
Instead, in lines 228-229 of the revised manuscript, there is still a reference to personal communication.
--> a proper ref. to Bronk Ramsey et al. 2020 has now been included

Similarly, I cannot find the reference to the abstract by Abé-Ouchi "for the OC3/IPODS Meeting held in Cambridge in September 2018"". Instead, in lines 656-657 of the revised manuscript, there is still a reference to personal communication. I suppose that in both cases the modifications to the manuscript were simply lost or forgotten. --> a proper ref. to Abé-Ouchi was now included.

(3) Length of manuscript

I am fine with your efforts to slightly shorten the abstract and the introduction. --> GREAT!

Finally, when reading your manuscript again it occurred to me that the model used by Gebbie (2014) is not the MIROC model, but a simple "water mass decomposition model" or "global tracer transport model", as the author himself calls it.
The paragraph leading up to line 653 of the revised version of the manuscript would need to be rephrased accordingly. --> To meet your argument our text at line 653 now was rephrased.

Yours sincerely,
André Paul
,,,

Plateaus and jumps in the atmospheric radiocarbon record – Potential origin and value as global age markers for glacial-to-deglacial paleoceanography, a synthesis

Michael Sarnthein[1)], Kevin Küssner[2)], Pieter M. Grootes[3)], Blanca Ausin[4)8)], Timothy Eglinton[8)], Juan Muglia[5)], Raimund Muscheler[6)], Gordon Schlolaut[7)]

1) Institute of Geosciences, University of Kiel, Olshausenstr. 40, 24098 Kiel, Germany, michael.sarnthein@ifg.uni-kiel.de, (corresponding author)
2) Alfred-Wegener-Institut Helmholtz-Zentrum für Polar- und Meeresforschung, Department for Marine Geology, 27570 Bremerhaven, Germany, kevin.kuessner@awi.de
3) Institute of Ecosystem Research, University of Kiel, Olshausenstr. 40, 24098 Kiel, Germany, pgrootes@ecology.uni-kiel.de
4) Geology Department, University of Salamanca, Plaza de los Caldos, 37008 Salamanca, Spain, <ausin@usal.es>
5) Centro para el Estudio de los Sistemas Marinos, CONICET, 2915 Boulevard Brown, U9120ACD, Puerto Madryn, Argentina, jmuglia@cenpat-conicet.gob.ar
6) Quaternary Sciences, Department of Geology Lund University, Sölvegatan 12, 22362 Lund, Sweden, raimund.muscheler@geol.lu.se
7) Climate Dynamics and Landscape Evolution, GFZ German Centre for Geosciences, Telegrafenberg, 14473 Potsdam, Germany, SchlolautG@gmail.com
8) Geological Institute, ETH Zürich, Sonneggstr. 5, 8092 Zuerich, Switzerland,

final version submitted to CLIMATE OF THE PAST (2020-08-8)

ABSTRACT

Changes in the geometry of ocean Meridional Overturning Circulation (MOC) are crucial in controlling past changes of climate and the carbon inventory of the atmosphere. However, the accurate timing and global correlation of short-term glacial-to-deglacial changes of MOC in different ocean basins still present a major challenge. The fine structure of jumps and plateaus in atmospheric and planktic radiocarbon (^{14}C) concentration reflects changes in atmospheric ^{14}C production, ocean-atmosphere ^{14}C exchange, and ocean mixing. Plateau boundaries in the atmospheric ^{14}C record of Lake Suigetsu, now tied to Hulu U/Th model-ages instead of optical varve counts, provide a stratigraphic 'rung ladder' of up to 30 age tie points 29 to 10 cal. ka for accurate dating of planktic oceanic ^{14}C records. The age differences between contemporary planktic and atmospheric ^{14}C plateaus record the global distribution of ^{14}C reservoir ages for surface waters of the Last Glacial Maximum (LGM) / deglacial Heinrich Stadial 1 (HS-1), as documented in 19/20 planktic ^{14}C records. Elevated and variable reservoir ages mark both upwelling regions and high-latitude sites covered by sea ice and/or meltwater. ^{14}C ventilation ages of LGM deep waters reveal opposed geometries of Atlantic and Pacific MOC. Like today, Atlantic deep-water formation went along with an estuarine inflow of old abyssal waters from the Southern Ocean up to the northern North Pacific and an outflow of upper deep waters. During early HS-1, ^{14}C ventilation ages suggest a reversed MOC and ~1500 year-long flushing of the deep North Pacific up to the South China Sea, when estuarine circulation geometry marked the North Atlantic, gradually starting near 19 ka. High ^{14}C ventilation ages of LGM deep waters reflect a major drawdown of carbon from the atmosphere. The subsequent major deglacial age drop reflects changes in MOC accompanied by massive carbon releases to the atmosphere as recorded in Antarctic ice cores. These new features of MOC and the carbon cycle provide detailed evidence in space and time to test and refine ocean models that, in part because of insufficient spatial model resolution and reference data, still poorly reproduce our data sets.

1. INTRODUCTION

1.1 A variety of terms linked to the notion '^{14}C age'

The ^{14}C concentration in the troposphere is mainly determined by ^{14}C production, atmospheric mixing, moreover, air-sea gas exchange and ocean circulation that vary over time (e.g., Alves et al., 2018; Alveson et al., 2018). The ^{14}C content of living terrestrial plants is in equilibrium with the atmosphere via processes of photosynthesis and respiration. Accordingly, the ^{14}C of terrestrial plant remains in a sediment section directly reflects the amount of radioactive decay, thus the time passed since the plant's death, and the ^{14}C composition of the atmosphere during the time of plant growth.

Contrariwise, ^{14}C values of marine and inland waters are cut off from cosmogenic ^{14}C production in the atmosphere, hence depend on the carbon transfer at the air-water interface and the result of local transport and mixing of carbon in the water. For surface waters, the air-sea transfer involves a time span of ten years and less (e.g., Nydal et al., 1998). Yet, vertical and horizontal water mixing results in surface ocean ^{14}C concentrations on average 5 % lower than those in the contemporaneous atmosphere, a difference expressed as 'Marine Reservoir Age' (or 'reservoir effect' *sensu* Alves et al., 2018). These 'ages' reflect the local oceanography and are highly variable through time (~200–2500 yr; e.g., Stuiver and Braziunas, 1993; Grootes and Sarnthein, 2006; Sarnthein et al., 2015). Apart from U/Th dated corals (many papers on their reservoir age since Adkins and Boyle, 1997), the ^{14}C age of planktic foraminifers is the most common tracer in marine sediments providing a rough estimate of the time passed since sediment deposition. Soon, however, marine geologists were confronted with age inconsistencies that implied a series of unknowns, in particular the surface ocean ^{14}C 'reservoir age' that finally became a most valuable tracer for oceanography.

The ^{14}C records of benthic foraminifers in deep-sea sediments reflect the time of radioactive decay since their deposition with the apparent 'ventilation age' of the deep waters in which they lived. Ventilation age is primarily the time span from the moment when carbon dissolved in the local surface waters with somewhat reduced ^{14}C level lost contact with the atmosphere until the precipitation of benthic carbonate from the down-welled deep waters. Details on the derivation of ventilation ages are provided in Cook and Keigwin (2015) and Balmer and Sarnthein (2018). In addition, however, ventilation ages include hardly quantifiable lateral admixtures of older and/or younger water masses, moreover, ^{14}C-enriched organic carbon supplied by the biological pump, thus are called 'apparent'. Today, the apparent transit times of carbon dissolved in the deep ocean range from a few hundred up to ~1800 ^{14}C yr found in upper deep waters of the northeastern North Pacific (Matsumoto, 2007).

The reservoir ages of surface waters and the ventilation ages of deep waters present robust and high-resolution tracers essential for drawing quantitative conclusions on past ocean circulation geometries, marine climate change, and the processes that drive both past ocean dynamics and carbon budgets, given the ages rely on a number of robust age tie points. Obtaining such tie points presents a problem, since any attempt to date a deep-sea sediment record by means of ^{14}C encounters a number of intricacies of how to disentangle the effects of global atmospheric ^{14}C variations due to past changes in cosmogenic ^{14}C production and carbon cycle from (i) local depositional effects such as sediment hiatuses and winnowing, differential bioturbational mixing depth, and sediment transport by deep burrows, (ii) the effects of local atmosphere-ocean exchange and ocean mixing resulting in reservoir and ventilation ages that change through time and

188 space (e.g., Alves et al. 2018; Grootes and Sarnthein, 2006), and (iii) from the final
189 target, quantitatively 'pure' ^{14}C ages due to radioactive decay. These problems are
190 exacerbated by the need for a generally accepted high-precision atmospheric reference
191 record for the period 14–50 cal. ka, beyond tree ring calibration,
192
193 Current ^{14}C-based chronologies of deep-sea sediment records, used to constrain and
194 correlate the age of glacial-to-deglacial changes in ocean dynamics and climate on a
195 global scale, are often of insufficient quality when they are based on (i) age tie points
196 spaced far too wide (e.g., using DO-events 1, 2, and 3 only and/or sporadic tephra
197 layers for the time span 30–14 cal ka), (ii) disregarding atmospheric ^{14}C plateaus, (iii)
198 the risky assumption of ±constant planktic ^{14}C reservoir ages and other speculative
199 stratigraphic correlations/compilations, and (iv) ignoring small-scale major differences in
200 low-latitude reservoir age. Likewise, clear conclusions are precluded by an uncertainty
201 range of 3-4 kyr sometimes accepted for tie points during the glacial-to-deglacial period
202 (Stern and Lisiecki, 2013; Lisiecki and Stern, 2016), where significant global climate
203 oscillations occurred on decadal-to-centennial time scales as widely shown on the basis
204 of speleothem and ice core-based records (Steffensen et al., 2008; Svensson et al.,
205 2008; Wang et al., 2001). Thus marine paleoclimate and paleoceanographic studies
206 today focus on the continuing quest for a high-resolution and global, hence necessarily
207 atmospheric ^{14}C reference record.
208
209 *1.2 Review of tie points used to fix calibrated and reservoir ages in marine ^{14}C records*
210 The tree ring-based calibration of ^{14}C ages provides a master record of decadal
211 changes in atmospheric ^{14}C concentrations back to ~14 cal. ka (Reimer et al., 2013 and
212 2020) with floating sections beyond (from ~12.5–14.5 cal. ka, around 29–31.5 and 43

213 cal. ka; Turney et al., 2010, 2017, Reimer et al., 2020). The evolution of Holocene and
214 late deglacial ^{14}C ages with time is not linear but reveals variations with numerous
215 distinct jumps (= rapid change) and (short) plateau-shaped (slow or no change or even
216 inversion) structures indicative of fluctuations in atmospheric ^{14}C concentration. Prior to
217 8500 cal. yr BP, various plateaus extend over 400–600 cal. yr and beyond (Fig. 2).
218 Given the quality of the tree ring calibration data, these fluctuations can be considered
219 real, suitable for global correlation (Sarnthein et al., 2007, 2015; Umling and Thunnell,
220 2017; Sarnthein and Werner, 2018). Air-sea gas exchange transfers the atmospheric
221 ^{14}C fluctuations into the surface ocean where they can provide high-resolution tie points
222 to calibrate the marine ^{14}C record and marine reservoir ages back to ~14 ka (via "^{14}C
223 wiggle matching"). In the near future, however, it is unlikely that a continuous tree ring-
224 based record will become available to trace such atmospheric ^{14}C variations further
225 back, over the period 14–29 cal. ka crucial for the understanding of last-glacial-to-
226 interglacial changes in climate. Hence various other, carbonate-based ^{14}C archives
227 have been employed for this period to reconstruct past changes in atmospheric ^{14}C
228 concentration/age and tie them to an ‘absolute’ or ’calibrated’ (e.g., incremental and/or
229 based on speleothem carbonate) age scale.
230
231 Suites of ^{14}C ages of paired marine and terrestrial plant-borne samples, e.g. paired
232 planktic foraminifers and wood chunks, provide most effective but rarely realizable
233 absolute-age markers and reservoir ages of local ocean surface waters (Zhao and
234 Keigwin, 2018; Rafter et al., 2018; Schroeder et al., 2016; Broecker et al., 2004).
235 Likewise successful appears the alignment of ^{14}C-dated variations in downcore sea-
236 surface temperatures (SST) with changes in hydroclimate as recorded in age-calibrated
237 sedimentary leaf-wax hydrogen isotope (δD) records from ancient lakes (Muschitiello et

al., 2019), assumed to be coeval. Further tie points are derived from volcanic ash layers (Waelbroeck et al., 2001; Siani et al, 2013; Davies et al., 2014; Sikes and Guilderson, 2016), paired U/Th- and ^{14}C-based coral ages (Adkins and Boyle, 1997; Robinson et al., 2005; Burke and Robinson, 2012; Chen et al., 2015), and the (fairly fragmentary) alignment of major tipping points in ^{14}C dated records of marine SST and planktic $\delta^{18}O$ to the incremental age scale of climate events dated in polar ice core records (Waelbroeck et al., 2011). Such well-defined tie points, however, are wide-spaced in peak glacial-to-early deglacial ice core records, too wide for properly resolving a clear picture of the spatiotemporal pattern of marine paleoclimate events. Finally, various data compilations tentatively rely on the use of multiple age correlations amongst likewise poorly dated marine sediment records, an effort necessarily problematic. Skinner et al. (2019) recently combined new and existing reservoir age estimates from North Atlantic and Southern Ocean to show coherent but distinct regional reservoir age trends in subpolar ocean regions, trends that indeed envelop the range of actual major small-scale and short-term oscillations in reservoir age revealed by our technique of ^{14}C plateau tuning for the subpolar South Pacific (Küssner et al., 2020 subm.).

Lacking robust age tie points several authors resort to ^{14}C reservoir age simulations for various sea regions by ocean General Circulation Models (GCM) (e.g. Butzin et al., 2017; Muglia et al., 2018) to quantify the potential difference between marine and atmospheric ^{14}C dates for glacial-to-interglacial times. In view of the complexity of ocean MOC and the global carbon cycle it is not surprising that the results of a comparison of a selection of robust empiric vs. simulated ^{14}C reservoir ages are not that encouraging yet (as discussed further below).

263 Beyond accepting a generally close link between ^{14}C concentrations in the troposphere
264 and in the surface ocean, the fine structure of planktic ^{14}C records with centennial-scale-
265 resolution can provide a far superior (though costly) link of the marine sediment records
266 to the reference suite of narrow-standing jumps and boundaries of the plateaus robustly
267 identified in the atmospheric ^{14}C record of Lake Suigetsu, the only long, continuous
268 record based on terrestrial plant remains (Bronk Ramsey et al., 2012, 2019). Beyond
269 the reach of the tree ring-based age scale ~14 cal. ka, the absolute age of the Suigetsu
270 atmospheric ^{14}C structures can be either calibrated by incremental (microscopy- or
271 XRF-based) varve counts (Schlolaut et al., 2018; Marshall et al., 2012) or by a series of
272 paired U/Th- and ^{14}C-based model ages correlated from the Hulu Cave speleothem
273 record (Bronk Ramsey, 2012 and 2019; Southon et al., 2012; Cheng et al., 2018). The
274 difference in absolute age between these calibrations (Fig. 3) is of little importance for
275 the tuning of planktic to corresponding atmospheric ^{14}C plateaus and the derivation of
276 planktic reservoir ages that present the highly variable offset of the ^{14}C age of a planktic
277 plateau from that of the correlated atmospheric plateau. The offset is deduced by
278 subtracting the average ^{14}C age of an atmospheric ^{14}C plateau from that of the
279 correlated planktic ^{14}C plateau, independent of any absolute age value assigned.
280
281 The uncertainty of the Suigetsu atmospheric 14C record is significantly larger than that
282 of the tree ring-based calibration record because of lower 14C concentrations, limited
283 sampling density, and uncertainties in the independent age determination. Thus the ^{14}C
284 fluctuations could be real or represent mere statistical scatter (null hypothesis) in which
285 case the record of atmospheric ^{14}C ages against time would show a simple continuous
286 rise resulting from radioactive decay and the advance of time, such as suggested by a

287 fairly straight progression of the highly resolved deglacial Hulu Cave ^{14}C record plotted
288 vs. U/Th ages (Southon et al., 2012; Cheng et al., 2018).
289
290 The unequivocal fluctuations in the tree ring-based master record of atmospheric ^{14}C
291 concentration (Fig. 2; Reimer et al., 2013, 2020) are on the order of 2–3 % over the last
292 10 kyr (Stuiver and Braziunas, 1993) and even larger back to ~14 ka. Under glacial and
293 deglacial low-CO_2 conditions beyond 14 ka, when climate and ocean dynamics were
294 less constant than during the Holocene, real atmospheric ^{14}C fluctuations were, most
295 likely, even stronger and ^{14}C plateaus and jumps accordingly larger. Plateau-jump
296 structures are also becoming increasingly evident in the evolving atmospheric
297 calibration record (Reimer et al., 2020). The age-defined plateaus and jumps in the
298 Suigetsu atmospheric ^{14}C calibration curve may thus be regarded as a suite of 'real'
299 structures, extending the calibration provided by the tree ring record for Holocene and
300 B/A-to-Early Holocene times (Fig. 2) into early deglacial and LGM times.
301
302 The plateau/jump structures may partly be linked to changes in cosmogenic ^{14}C
303 production, as possibly shown in the ^{10}Be record (Fig. 4; based on data of Adolphi et al.,
304 2018), and – presumably more dominant – to short-term changes in ocean mixing and
305 the carbon exchange between ocean and atmosphere. The exchange is crucial, since
306 the carbon reservoir of the ocean contains up to 60 (preindustrial) atmospheric carbon
307 units (Berger and Keir, 1984). The apparent contradiction with the smooth Hulu Cave
308 ^{14}C record (Southon et al., 2012; Cheng et al., 2018) may possibly be explained by the
309 Hulu Cave speleothem precipitation system acting as a low-pass filter for fluctuating
310 atmospheric ^{14}C concentrations (statistical tests of Bronk Ramsey et al., 2020) and, to a
311 very limited degree, by the obvious scatter in the Suigetsu data. The filter for Hulu data

312 possibly led to a loss especially of short-lived structures in the preserved atmospheric
313 ^{14}C record, though some remainders were preserved in the ^{14}C records of Hulu Cave
314 (Fig. 1). So we rather trust the amplitude of Suigetsu ^{14}C structures than the timing of
315 Hulu Cave data.
316
317 Like a 'rung ladder' the age-calibrated suite of ^{14}C plateau boundaries and jumps is
318 suited for tracing the calibrated age of numerous plateau boundaries in glacial-to-
319 deglacial marine ^{14}C records likewise densely sampled, even when some rungs have
320 been destroyed by local influences on gas exchange or ocean mixing. Also, one may
321 record the average offset of planktic ^{14}C ages from paired atmospheric ^{14}C ages, i.e. the
322 planktic reservoir age, for each single ^{14}C plateau (Sarnthein et al., 2007, 2015). We
323 prefer the Suigetsu record to IntCal, since it is based on original primary atmospheric
324 data and results in small-scale spatio-temporal changes of reservoir age, whereas
325 IntCal is mixing and smoothing a broad array of different data sources with comparativ-
326 ely coarse age resolution, including carbonate-based speleothem and marine records.
327 For the first time, this suite of tie points may facilitate a precise temporal correlation of
328 all sorts of changes in surface and deep-water composition on a global scale, crucial for
329 a better understanding of past changes in ocean and climate dynamics.
330
331 *1.3 Items discussed in this synthesis*
332 The Results Section is summarizing (1) Means to separate noise, global atmospheric
333 and local oceanic forcings that together control the structure of a planktic ^{14}C plateaus,
334 (2) The choice of a U/Th-based reference time scale (Bronk Ramsey et al. 2012; Cheng
335 et al., 2018) instead of the earlier varve-counted version (Schlolaut et al., 2018) to date
336 the structures in the global atmospheric ^{14}C record of Lake Suigetsu (Sarnthein et al.,

337 2015), (3) The extension of the suite of age tie points from 23 back to 29 cal. ka, values
338 crucial for an accurate global correlation of ocean events over the Last Glacial
339 Maximum, and (4) Potential linkages of atmospheric ^{14}C plateaus and jumps to
340 cosmogenic ^{14}C production and/or ocean dynamics.
341
342 The Discussion and Implications section includes:
343 (1) A global summary of published marine ^{14}C reservoir age records (Sarnthein et al.
344 2015) now enlarged by nine plateau-tuned records from the Southern Hemisphere
345 (Balmer et al., 2016 and 2018; Küssner et al., 2018 and 2020 subm.) and the northeast
346 Atlantic (Ausin et al., 2020 subm.). In total, 18 (LGM) / 19 (HS-1) plus three wood
347 chunk-based records (Broecker et al., 2004; Zhao et al., 2018) now depict the spatio-
348 temporal variability of past reservoir ages of surface waters in different ocean regions.
349 (2) A comparison of our plateau-based reservoir ages with LGM estimates of surface
350 water ^{14}C reservoir ages simulated by the GCM of Muglia et al. (2018).
351 (3) More detailed insights into the origin of past changes in the global carbon cycle from
352 glacial to interglacial times are provided by the enlarged set of ^{14}C reservoir and venti-
353 lation ages that form a robust tracer of global circulation geometries and the inorganic
354 carbon (DIC) dissolved in different basins of the ocean (Sarnthein et al., 2013).
355
356 The discussion highlights ^{14}C plateau tuning and its revised cal. time scale for global
357 data-model intercomparison and a new understanding of Ocean MOC during the LGM
358 and its reversal during HS-1.
359
360 2. RESULTS – AGE TIE POINTS BASED ON ^{14}C PLATEAU BOUNDARIES
361

362 2.1 *Suite of planktic ^{14}C plateaus: Means to separate global atmospheric from local*
363 *oceanographic forcings*
364 The basic assumption of the ^{14}C plateau tuning technique is that the fine structure of
365 fluctuations of the global atmospheric ^{14}C concentration record can also be found in the
366 surface ocean. In a plot of ^{14}C age versus calendar age such fluctuations lead to a pattern
367 of plateaus/jumps that correspond to decreases/increases in ^{14}C concentration. Here we
368 refer to the derivation and interpretation of planktic ^{14}C plateaus, assuming a predom-
369 inantly global atmospheric origin with occasional local oceanographic forcings. The series
370 of planktic ^{14}C plateaus and jumps are derived in cores with average hemipelagic
371 sedimentation rates of >10 cm/ky and dating resolution of <100-150 yr. The plateau-
372 specific structures in a sediment age-depth record form a well-defined suite for which
373 absolute age and reservoir age are derived by means of a strict alignment to the reference
374 suite of global atmospheric ^{14}C plateaus as a whole. Initially, age tie points of planktic
375 foraminiferal $\delta^{18}O$ records showing (orbital) isotope stages #1-3 serve as stratigraphic
376 guideline for the alignment under the simplifying assumption that stratigraphic gaps are
377 absent, not always true (Suppl. Fig. 2). Planktic reservoir ages and their short-term
378 changes are derived from the difference in average ^{14}C age between atmosphere and
379 surface waters in subsequent plateaus. To stick as close as possible to the modern range
380 of reservoir ages (Stuiver and Braziunas, 1993), tuned reservoir ages are kept at a
381 minimum unless stringent evidence requires otherwise.
382
383 A close correspondence between ^{14}C concentrations in atmosphere and surface ocean
384 is expected based on rapid gas exchange. In several cases, however, the specific
385 structure and relative length of a planktic ^{14}C plateau may deviate from those of the
386 pertinent plateau observed within the suite of atmospheric plateaus, thus indicate local

387 intra-plateau changes of reservoir age. Though less frequent, these changes may indeed
388 amputate and/or deform a plateau, then as result of variations in local ocean atmosphere
389 exchange and oceanic mixing. Two aspects help to sort out short-term climate-driven
390 intra- and inter-plateau changes in ^{14}C reservoir age: (i) The evaluation of the structure
391 and reservoir age of an individual plateau is strictly including the age estimates deduced
392 for the complete suite of plateaus. (ii) Our experience shows that deglacial climate
393 regimes in control of changes in surface ocean dynamics generally occurred on (multi-)
394 millennial time scales (e.g., YD, B/A, HS-1), whereas atmospheric ^{14}C plateaus hardly
395 lasted longer than a few hundred up to 1100 yr (Fig. 1 and S1). Abrupt changes in gas
396 exchange or ocean mixing usually affect one or only a few plateaus of the suite. --
397 Absolute age estimates within a plateau are derived by linear interpolation between the
398 age of the base and top of an undisturbed plateau assuming constant sedimentation
399 rates. The potential impact of short-term sedimentation pulses on ^{14}C plateau formation
400 has largely been discarded by Balmer and Sarnthein (2016).
401
402 *2.2 Suigetsu atmospheric ^{14}C record: Shift to a chronology based on U/Th model ages*
403 Originally, we based the chronology of ^{14}C plateau boundaries in the Suigetsu record
404 (Sarnthein et al., 2015) on a scheme of varve counts by means of light microscopy of
405 thin sections (Bronk Ramsey et al., 2012; Schlolaut et al., 2018). Over the crucial
406 sediment sections of the Last Glacial Maximum (LGM) and deglacial Heinrich Stadial 1
407 (HS-1), however, varve quality / perceptibility in the Suigetsu profile is highly variable
408 (Fig. 5). In parallel, varve-based age estimates were derived from counting various
409 elemental peaks in μXRF data and interpreted as seasonal signals (Marshall et al.,
410 2012). The results obtained from the two independent counting methods and their
411 interpolations widely support each other but diverge for older ages. The varve counts

412 ultimately formed the backbone of a high-resolution chronology obtained by tying the
413 Suigetsu ^{14}C record to the U/Th based time scale of the Hulu cave ^{14}C record (Bronk
414 Ramsey et al., 2012). Recently, Schlolaut et al. (2018) amended the scheme of varve
415 counts. Accordingly, Suigetsu varve preservation (i.e., the number of siderite layers per
416 20 cm thick sediment section) is fairly high prior to ~32 ky BP and over late glacial
417 Termination I but fairly poor over large parts of the LGM and HS-1, from ~15 – 32 cal ka
418 (17.3-28.5 m c.d. in Fig. 5). Here only less than 20-40 % of the annual layers expected
419 from interpolation between clearly varved sections are distinguished by microscopy.
420 Varve counts that use µXRF data (Marshall et al., 2012) can distinguish subtle changes
421 in seasonal element variations, that are not distinguishable in thin section microscopy,
422 hence result in higher varve numbers especially during early deglacial-to-peak glacial
423 times. Yet, some subtle variations are difficult to distinguish from noise, which adds
424 uncertainty to the µXRF-based counts. Thus, the results from either counting method
425 are subject to uncertainties that rise with increased varve age (Fig. 5).
426
427 Bronk Ramsey et al. (2012) established a third time scale based on ^{14}C wiggle matching
428 to U/Th dated ^{14}C records of the Hulu Cave and Bahama speleothems. In part, this
429 calibrated (cal.) age scale was based on Suigetsu varve counts, in part on the
430 prerequisite of the best-possible fit of a pattern of low-frequency changes in ^{14}C
431 concentration obtained from Suigetsu and Hulu Cave. The two ^{14}C records were fitted
432 within the uncertainty envelope of the Hulu 'Old / Dead Carbon Fraction' (OCF/DCF) of
433 ^{14}C concentration. The uncertainty of this model is still incompletely understood. The
434 U/Th-based age model of Suigetsu may suffer from the wiggle matching of atmospheric
435 ^{14}C ages of Lake Suigetsu with ^{14}C ages of the Hulu Cave (Southon et al., 2012) in case
436 of major short-term changes in atmospheric ^{14}C concentration due to a memory effect of

soil organic carbon in carbonate-free regions of the cave overburden. The speleothem-carbonate-based Hulu ages may have been influenced far more strongly by short-term changes in the local DCF than assumed, as suggested by major variations in a paired $\delta^{13}C$ record, that reach up to 5 ‰, mostly subsequent to short-term changes in past monsoon climate (Kong et al., 2005). The uncertainty regarding the assumption of a constant OCF/DCF (Southon et al. 2012; Cheng et al., 2018) may hamper the age model correlation between Hulu and Suigetsu records and the Suigetsu chronology.

We compared the results of the two timescales, independently deduced from varve counts, with those of the U/Th-based model age scale using as test case the base of ^{14}C Plateau 2b, the oldest tie point constrained by μXRF-based counts. In contrast to 16.4 cal. ka, supposed by optical varve counts, μXRF-based counts suggest an age of ~16.9 cal. ka (Marshall et al., 2012; Schlolaut et al., 2018), which matches closely the U/Th-based estimate of 16.93 ka. This is a robust argument for the use of the U/Th-based Suigetsu time scale as 'best possible' age scale to calibrate the age of thirty ^{14}C plateau boundaries (Fig. 1). In its older part, the U/Th model time scale is further corroborated by a decent match of short-term increases in ^{14}C concentration with the low geomagnetic intensity of the Mono Lake and Laschamp events at ~34 and 41.1±0.35 ka (Lascu et al., 2016), independently dated by other methods. The new U/Th-based model ages of ^{14}C plateau boundaries are significantly higher than our earlier microscopy-based varve ages over HS-1 and LGM, a difference increasing from ~200 yr near 15.3 cal. ka to ~530 near 17 ka and 2000 yr near ~29 ka (Fig. 3).

Note, any readjustment of the calendar age of a ^{14}C plateau boundary does not entail any change in ^{14}C reservoir ages afore deduced for surface waters by means of the

462 plateau technique (Sarnthein et al., 2007, 2015), since each reservoir age presents the
463 simple difference in average ^{14}C age for one and the same ^{14}C plateau likewise defined
464 in both the Suigetsu atmospheric and planktic ^{14}C records of marine surface waters,
465 independent of the precise position of this plateau on the calendar age scale.
466
467 In view of the recent revision of time scales (Schlolaut et al., 2018; Bronk Ramsey et al,
468 2019) we now extended our plateau tuning and now also defined the boundaries and
469 age ranges of ^{14}C plateaus and jumps for the interval ~23–29 cal. ka, which results in a
470 total of ~30 atmospheric age tie points for the time span 10.5–29 cal. ka (Fig. 1;
471 summary in Table 1; following the rules of Sarnthein et al., 2007 and 2015). Prior to 25
472 cal. ka, the definition of ^{14}C plateaus somewhat suffered from an enhanced scatter of
473 raw ^{14}C values of Suigetsu. -- In addition to visual inspection, the ^{14}C jumps and
474 plateaus were also defined with higher statistical objectivity by means of the first-
475 derivative of all trends in the ^{14}C age-to-calendar age relationship (or –core depth
476 relationship, respectively) by using a running kernel window (Sarnthein et al., 2015).
477
478 *2.3 Linkages of short-term structures in the atmospheric ^{14}C record to changes in*
479 *cosmogenic ^{14}C production versus changes in ocean dynamics*
480
481 Potential sources of variability in the atmospheric ^{14}C record have first been discussed
482 by Stuiver and coworkers in the context of Holocene fluctuations deduced from tree ring
483 data (e.g., Stuiver and Braziunas 1993), more recently simulated (e.g., Hain et al.,
484 2014). -- Similar to changes in ^{14}C, variations in ^{10}Be deposition in ice cores reflect past
485 changes in ^{10}Be production as a result of changes in solar activity and the strength of
486 the Earth's magnetic field (Adolphi et al., 2018). If we accept to omit assumptions on the

487 modulation of past ^{14}C concentrations by changes in the global carbon cycle we can
488 calculate the atmospheric ^{14}C changes over last glacial-to-deglacial times with ^{10}Be and
489 a carbon cycle model and convert them into ^{14}C ages (Fig. 4). Changes in climate and
490 carbon cycle, however, over this period necessarily modified the ^{10}Be-based ^{14}C record
491 if included correctly into the modeling. Between 10 and 13.5 cal. ka, the ^{10}Be-modeled
492 ^{14}C record displays a number of plateau structures that appear to match the Suigetsu-
493 based atmospheric ^{14}C plateaus. Between 15 and 29 cal. ka, however, ^{10}Be-based ^{14}C
494 plateaus are more rare and/or less pronounced than those in the Suigetsu record. Most
495 modelled plateaus are far shorter than those displayed in the suite of atmospheric ^{14}C
496 plateaus of Lake Suigetsu (e.g., plateaus near to the top 2a, 2b, top 5a, and 9), except
497 for a distinct equivalent of plateau no. 6a. On the whole, the modelled and observed
498 structures show little coherence. This may indicate that any direct relationship between
499 variations in cosmogenic ^{14}C production and the Suigetsu plateau record is largely
500 obscured by the carbon cycle, uncorrected climate effects on the ^{10}Be deposition,
501 and/or noise in the ^{14}C data. Also, a relatively high uncertainty of the measured ^{10}Be
502 concentrations in the ice, (in many cases ~7%; Raisbeck et al., 2017), and a lower
503 sample resolution in the order of 50 to 200 yr may contribute to the smoothed character
504 of the ^{10}Be record in Fig. 4.
505
506 On the other hand, the 'new' U/Th-based cal. ages of plateau boundaries may suggest
507 some reasonable stratigraphic correlations between peak glacial and deglacial change in
508 atmospheric CO_2 and ^{14}C plateaus with millennial-scale events in paleoceanography (Fig.
509 6, Table 2): The suite of deglacial ^{14}C plateaus no. 2a, 1, and Top YD indeed displays a
510 temporal match with three brief but major deglacial jumps in ocean degassing of CO_2
511 documented in the WDC ice core (Marcott et al., 2014). The two records have been

512 independently dated by means of annual-layer counts in ice cores and U/Th ages of
513 stalagmites. The match suggests that these atmospheric ^{14}C plateaus may largely result
514 from changes in air-sea gas exchange, and in turn, from changes in ocean dynamics.
515
516 In particular, these events may have been linked to a variety of fast changes such as in
517 sea ice cover in the Southern Ocean and/or in the salinity and buoyancy of high-latitude
518 surface waters (Skinner et al., 2010; Burke and Robinson, 2012). These factors control
519 upwelling and meridional overturning of deep waters, in particular found in the Southern
520 Ocean (Chen et al., 2015) and/or North Pacific (Rae et al. 2014, Gebhardt et al., 2008).
521 Such events of changes in MOC geometry and intensity may be responsible for ocean
522 degassing and the ^{14}C plateaus. The enhanced mixing of the Southern Ocean and a
523 similar, slightly later mixing event in the North Pacific (MD02-2489; Fig. S2d) may have
524 triggered – with phase lag – two trends in parallel, (1) a rise in atmospheric CO_2, in part
525 abrupt (*sensu* Chen et al., 2015; Menviel et al., 2018), and (2) a gradual enrichment in ^{14}C
526 depleted atmospheric carbon, reflected as ^{14}C plateau.
527
528 Plateau 6a matches a ^{14}C plateau deduced from atmospheric ^{10}Be concentrations, thus
529 suggests changes in ^{14}C production. Other changes in atmospheric ^{14}C (plateaus 4 and
530 8) match short-term North Atlantic warmings during peak glacial and earliest deglacial
531 times, similar to that at the end of HS-1 and during plateau 'YD', hence may reflect
532 minor changes in ocean circulation and ocean-atmosphere exchange without major
533 degassing of old ^{14}C depleted deep waters in the North Atlantic (Table 2, Fig. S2a).
534 There is still little information, however, on the origin of several other peak glacial ^{14}C
535 plateaus 17.5–29 cal. ka. The actual linkages of these plateaus to events in ocean MOC
536 still remain to be uncovered.

3. DISCUSSION and IMPLICATIONS

3.1 ^{14}C plateau boundaries – A suite of narrow-spaced age tie points to rate short-term changes in marine sediment budgets, chemical inventories, and climate 29–10 cal. ka

In continuation of previous efforts (Sarnthein et al., 2007 and 2015) the tuning of high-resolution planktic ^{14}C records of ocean sediment cores to the new age-calibrated atmospheric ^{14}C plateau boundaries now makes it possible to establish a 'rung ladder' of ~30 age tie points covering the time span 29 – 10 cal. ka. These global tie points have a time resolution of several hundred to thousand years to be used to constrain the chronology and potential leads and lags of events that occurred during peak glacial and deglacial times (Fig. 1). The locations of 18 (20; depending on the age range covered) ^{14}C records are shown in Fig. 7. Figs. 8 and S2 give the time histories of the planktic and benthic reservoir ages, the information they provide is discussed below.

Six prominent examples showing the power and value of additional information obtained by means of the ^{14}C plateau-tuning method are:

(i) The timing of ocean signals of the onset of deglaciation (sudden depletion of planktic $\delta^{18}O$ and rise in SST) in the North Atlantic and North Pacific can now be distinguished in detail from those in the Southern Hemisphere, where warming began at 17.6 cal. ka, when the cooling of Heinrich 1 started in the North Atlantic (Fig. S2) (Küssner et al., 2020 subm.); in harmony with Schmittner and Lund, 2015), a finding important to further constrain global 'bipolar see-saw' (Stocker and Johnsen, 2003).

(ii) Likewise, the end of the cooling equated with the Antarctic Cold Reversal (ACR; WDC Project Members, 2013) in Pacific surface waters off Central Chile was found

562 precisely coeval with the onset of the Younger Dryas cold spell in the Northern
563 Hemisphere (Küssner et al., 2020 subm.).
564 (iii) Signals of local deep-water formation in the subpolar North Pacific can now be
565 separated from signals originating in the North Atlantic (Rae et al. 2014; Sarnthein et al.,
566 2013). In this way we now can specify and tie major short-lasting reversals in Atlantic
567 and Pacific MOC on a global scale.
568 (iv) Signals of deglacial meltwater advection can now be distinguished from short-
569 term interstadial warmings in the northern subtropical Atlantic, which helps to locate
570 meltwater outbreaks far beyond the well-known Heinrich belt of ice-rafted debris
571 (Balmer and Sarnthein, 2018).
572 (v) As outlined above, the timing of marine ^{14}C plateaus can now be compared in
573 detail with that of deglacial events of climate and the atmospheric CO_2 rise independ-
574 ently dated by means of ice core-based stratigraphy (Table 2; Fig. 6). These linkages
575 offer a tool to explore details of deglacial changes in deep-ocean MOC once the suite of
576 ^{14}C plateaus has been properly tuned at any particular ocean site.
577 (vi) The refined scale of age tie points also reveals unexpected details for changes in
578 the sea ice cover of high latitudes as reflected by anomalously high ^{14}C reservoir ages
579 (e.g. north of Iceland and near to the Azores Islands) and for the evolution of Asian
580 summer monsoon in the northern and southern hemisphere as reflected by periods of
581 reduced sea surface salinity (e.g., Sarnthein et al., 2015; Balmer et al., 2018).
582
583 Finally, the plateau-based high-resolution chronology has led to the detection of
584 numerous millennial-scale hiatuses (e.g., Sarnthein et al., 2015; Balmer et al., 2016;
585 Küssner et al., 2020 subm.) overlooked by conventional, e.g., *AnalySerie*-based
586 methods (Paillard et al. 1996) of stratigraphic correlation (Fig. S2). In turn, the hiatuses

give intriguing new insights into past changes of bottom current dynamics linked to different millennial-scale geometries of overturning circulation and climate change such as in the South China Sea (Sarnthein et al., 2013 and 2015), in the South Atlantic (Balmer et al. 2016) and southern South Pacific (Ronge et al., 2019).

Clearly, the new atmospheric ^{14}C 'rung ladder' of closely-spaced chronostratigraphic tie points has evolved to a valuable tool to uncover functional chains in paleoceanography, that actually have controlled events of climate change over glacial-to-deglacial times. The extension of the age range back to 29 ka allows constraining potential changes in the ocean dynamics expected for Dansgaard Oeschger (DO) events 2, 3, and 4 as compared to those found for DO-1, though pertinent core records are still missing.

3.2 Observed vs. model-based ^{14}C reservoir ages that act as tracer of past changes in surface ocean dynamics provide incentive for model refinements

Radiocarbon plateau tuning of marine sediment sections to the Suigetsu ^{14}C atmospheric master record allows us to establish at semi-millennial-scale resolution the difference between the average ^{14}C age of coeval atmospheric and planktic ^{14}C plateaus. The suite of changing ^{14}C reservoir ages over time forms a prime tracer of past ocean dynamics influencing local surface waters and a data set crucial to deduce past apparent deep-water ventilation ages (e.g., Muglia et al., 2018; Cook and Keigwin, 2015; Balmer and Sarnthein, 2018).

To better constrain the water depth of past reservoir ages we dated monospecific planktic foraminifera (Sarnthein et al., 2007); in low-to-mid latitudes on *G. bulloides*, *G.*

612 *ruber,* or *G. sacculifer* with habitat depths of 0–80/120 m (Jonkers and Kucera, 2017)
613 and in high latitudes, mostly on *N. pachyderma* (s) living at 0–200 m depth (Simstich et
614 al., 2003). Averaging of ^{14}C ages within a ^{14}C plateau helps to remove analytical noise
615 and minor real ^{14}C fluctuations. Nine plateaus are located in the LGM, 18–27 cal. ka
616 (Fig. 1). Here, planktic foraminifera-based reservoir ages show analytical uncertainties
617 of >200 to >300 yr each for standard AMS dating. By comparison, short-term temporal
618 variations in reservoir age reach 200–400 yr, occasionally up to 600 yr, in particular,
619 close to the end of the LGM (Table 3).
620
621 To better decode the informative value of our ^{14}C reservoir ages for late LGM we
622 compared average ages of ^{14}C Plateaus 4-5 (18.6–20.9 cal. ka) with estimates
623 generated by various global ocean models, an approach similar to that of Toggweiler et
624 al. (2019) applied to modern reservoir ages of the global ocean. In an earlier paper
625 (Balmer et al., 2016) we compared our empiric reservoir ages for the LGM with GCM-
626 based estimates of Franke et al. (2008) and Butzin et al. (2012). Franke et al. (2008)
627 underestimated our mid-latitude values by up to ~2000 ^{14}C yr, while LGM reservoir age
628 estimates of Butzin et al. (2012) were more consistent with ours. Their GCM
629 considered more realistic boundary conditions such as the LGM freshwater balance in
630 the Southern Ocean and, in particular, LGM SST and wind fields plus the gas transfer
631 velocity for the exchange of ^{14}C of CO_2 (Sweeney et al., 2007). Further improvements
632 are expected from a model configuration that properly resolves the topographic details
633 of the continental margins and adjacent seas, which frequently form the origin of our
634 sediment-based data sets (Butzin et al., 2020). For the time being, we compared our
635 empirical estimates with estimates from a coarse-resolution GCM, using the results by
636 Muglia et al. (2018; 0–50 m w.d.; Fig. 8c-d; Table 3) as an example. Their model

637 includes ocean surface reservoir age and ocean radiocarbon fields that have been
638 validated through a comparison to LGM ^{14}C data compilation made by Skinner et al.
639 2017. It conforms two plausible, recent model estimates of surface reservoir ages that
640 can be compared to our results (Table 3).
641
642 Low LGM values (300–750 yr) supposedly document an intensive exchange of surface
643 waters with atmospheric CO_2, most common in model- and foraminifera-based
644 estimates of the low- and mid-latitude Atlantic. Low empiric values also mark LGM
645 waters in mid to high latitudes off Norway and off middle Chile, that is, close to sites of
646 potential deep and/or intermediate water formation. Off Norway and in the northeastern
647 Atlantic, model-based reservoir ages of Muglia et al. (2018) largely match the empiric
648 range. However, the uncertainty envelopes for data shown in Fig. 8c (±560 yr; r = 0.59)
649 generally exceed by far the spatial differences calculated for the empiric data.
650 Conversely, model-based reservoir ages reproduce only poorly the low planktic
651 foraminifera-based estimates off Central Chile and values in the Western Pacific and
652 Southern Ocean.
653 In part, the differences may be linked to problems like insufficient spatial resolution
654 along continental margins, ignoring east-west differences within ocean basins, and/or
655 the estimates of a correct location and extent of seasonal sea ice cover used as LGM
656 boundary condition such as east off Greenland, in the subpolar northwest Pacific, and
657 off Southern Chile, where sea ice hindered the exchange of atmospheric carbon (per
658 analogy to that of temperature exchange, e.g., Sessford et al, 2019). Also, model
659 estimates of the annual average are compared to ^{14}C signals of planktic foraminifera
660 that mostly formed during summer only, e.g., when large parts of the Nordic Seas were

661 found ice-free (Sarnthein et al., 2003). Hence, models may need to better constrain
662 local and seasonal sealing effects of LGM sea ice cover.
663
664 In general, the foraminifera-based reservoir age estimates for our sites that represent
665 various hydrographic key regions in the high-latitude ocean appear much higher than
666 model-derived values. These deviations reach up to 1400 yr, in particular in the
667 Southern Ocean. In part, they may result from the fact that present models may not yet
668 be suited to capture small-scale ocean structures such as the interference of ocean
669 currents with local bathymetry and local upwelling cells. Here, model-based reservoir
670 ages appear far too low in LGM regions influenced by regional upwelling such as the
671 South China Sea then governed by an estuarine overturning system (Wang et al., 2005;
672 Fig. 9), by coastal upwelling off N.W. Australia (Xu et al., 2010; Sarnthein et al., 2011),
673 or by a melt water lid such as off eastern New Zealand (Bostock et al., 2013; Küssner et
674 al., 2020 subm.). Local oceanic features are likely to be missed in current resolution
675 models. Our more narrow-spaced empiric data could help to refine the skill of models to
676 capture past ^{14}C reservoir ages.
677
678 Various differences amongst plankton- and model-based reservoir ages may also result
679 from differential seasonal habitats of the different planktic species analyzed that, in turn,
680 may trace different surface and subsurface water currents. Distinct interspecies
681 differences were found in Baja California that record differential, upwelling-controlled
682 habitat conditions (Lindsay et al, 2015). In the northern Norwegian Sea interspecies
683 differences amount up to 600 yr for the Preboreal ^{14}C plateau, 9.6–10.2 cal. ka
684 (Sarnthein and Werner, 2018). Here ^{14}C records of Arctic *Turborotalita quinqueloba*,
685 dominantly grown close to the sea surface during peak summer, differ from the paired

686 record of *Neogloboquadrina pachyderma*, formed in subsurface waters, and that of
687 subpolar species *N. incompta*, mainly advected from the south by Norwegian Current
688 waters well mixed with the atmosphere during peak winter. This makes closer
689 specification of model results as product of different seasonal extremes a further target.
690
691 *3.3 Planktic foraminifera-based ^{14}C reservoir ages – A prime database to estimate past*
692 *changes in the ^{14}C ventilation age of deep waters and past oceanic MOC and DIC*
693
694 'Raw' apparent benthic ventilation ages (in ^{14}C yr; 'raw' *sensu* Balmer et al., 2018)
695 express the difference between the (coeval) atmospheric and benthic ^{14}C levels
696 measured at any site and time of foraminifer deposition. These ages are the sum of (1)
697 the planktic reservoir age of the ^{14}C plateau that covers a group of paired benthic and
698 planktic ^{14}C ages and (2) the (positive or negative) ^{14}C age difference between any
699 benthic ^{14}C age and the average ^{14}C age of the paired planktic ^{14}C plateau. The benthic
700 ventilation ages necessarily rely on the high quality of ^{14}C plateau-based chronology,
701 since the atmospheric ^{14}C level has been subject to substantial short-term changes over
702 glacial-to-deglacial times. Necessarily, the ventilation ages include a mixing of different
703 water masses that might originate from different ocean regions and may contribute
704 differential ^{14}C ventilation ages, an unknown justifying the modifier 'apparent'.
705
706 In a further step, the $\Delta\Delta^{14}C$ equivalent of our 'raw' benthic ventilation age may be
707 adjusted to changes in atmospheric ^{14}C that occurred over the (short) time span
708 between deep-water formation and benthic sediment deposition (e.g., Balmer and
709 Sarnthein, 2018; Cook and Keigwin, 2015). In most cases, however, this second step is

710 omitted since its application usually does not imply any major modification of the
711 ventilation age estimates (Fig. S2a; Skinner et al., 2017; Sarnthein et al., 2013).
712
713 On the basis of ^{14}C plateau tuning we now can rely on 18 accurately dated records of
714 apparent benthic ^{14}C ventilation ages (Fig. S2a-d) to reconstruct the global geometry of
715 LGM and HS-1 deep and intermediate water circulation as summarized in ocean
716 transects and maps (Figs. 9–11) and discussed below. The individual matching of our
717 20 planktic ^{14}C plateau sequences with that of the Suigetsu atmospheric ^{14}C record is
718 displayed in Sarnthein et al. (2015), Balmer et al., (2016), Küssner et al. (2020 subm.),
719 and Ausin et al. (2020 subm.). In addition, robust estimates of past reservoir ages are
720 obtained for 4 planktic and benthic ^{14}C records from paired atmospheric ^{14}C ages of
721 wood chunks (Rafter et al., 2018; Zhao and Keigwin, 2018; Broecker et al., 2004).
722
723 *3.3.1 — Major features of ocean meridional overturning circulation during LGM (Fig. 10)*
724
725 Off Norway and near the Azores Islands very low benthic ^{14}C ventilation ages of <100–
726 750 yr suggest ongoing deep-water formation in the LGM northern North Atlantic
727 reaching down to more than 3000–3500 m water depth, with a flow strength possibly
728 similar to today (and a coeval deep countercurrent of old waters from the Southern
729 Ocean flowing along the East Atlantic continental margin off Portugal). This pattern
730 clearly corroborates the assembled benthic $\delta^{13}C$ record showing plenty of elevated $\delta^{13}C$
731 values for the northwestern, eastern and central North Atlantic (Sarnthein et al., 1994;
732 Millo et al., 2006; Keigwin and Swift, 2017). Irrespective of unspecified potential zonal
733 variations in deep-water ventilation age at mid latitudes and different from a number of
734 published models (e.g., Ferrari et al., 2014; Butzin et al., 2017) this ‘anti-estuarine’

735 pattern has been confirmed by a global tracer transport model of Gebbie (2014),
736 MIROC model simulations (Sherriff-Tadano et al., 2017, Yamamoto et al., 2019), and
737 independently, by ε_{Nd} records (Howe et al., 2016; Lippold et al., 2016). The latter
738 suggest an overturning of AMOC possibly even stronger than today, in particular due to
739 a 'thermal threshold' (Abé-Ouchi, 2018) overlooked in other model simulations.
740
741 In contrast to the northern North Atlantic, deep waters in the southern North Atlantic and
742 Circumpolar (CP) deep waters in the subpolar South Atlantic show an LGM ^{14}C
743 ventilation age of ~3640 yr, finally rising up to 3800 yr (Figs. 10, 11, S2b). These waters
744 were upwelled and admixed from below to surface waters near to the sub-Antarctic
745 Front during terminal LGM (Fig. S2b; Skinner et al., 2010; Balmer and Sarnthein, 2016;
746 model of Butzin et al., 2012).
747
748 In the southwestern South Pacific abyssal, in part possibly Antarctic-sourced waters
749 (Rae and Broecker, 2018) likewise show high apparent ^{14}C ventilation ages of 3500 yr
750 that drop to 2750 yr near the end of the LGM (Figs. 10 top and S2c) (^{14}C dates of
751 Ronge et al., 2016, modified by planktic ^{14}C reservoir ages of Küssner et al., 2020
752 subm.). A vertical transect of benthic $\delta^{13}C$ (McCave et al., 2008) suggests that the
753 abyssal waters were overlain by CP waters, separated by pronounced stratification near
754 ~3500–4000 m water depth. In part, the CP waters stemmed from North Atlantic Deep
755 Water. Probably, their apparent ventilation age 3500 yr came close to the values found
756 in the southern South Atlantic. East of New Zealand the CP waters entered the deep
757 western Pacific and spread up to the subpolar North Pacific, where LGM ^{14}C ventilation
758 ages reached ~3700 yr, possibly occasionally 5000 yr (Fig. S2d).
759

760 Similar to today, the MOC of the LGM Pacific was shaped by estuarine geometry,
761 probably more weakened than today (Du et al., 2018) and more distinct in the far
762 northwest than in the far northeast. This geometry resulted in an upwelling of old deep
763 waters in the subarctic Northwest Pacific, here leading to a ^{14}C reservoir age of ~1700
764 yr for surface waters at terminal LGM. On top of the Lower Pacific Deep Waters we may
765 surmise Upper Pacific Deep Waters that moved toward south (Figs. 10 top and 11).
766
767 The Pacific deep waters were overlain by Antarctic / Pacific Intermediate Waters (IW)
768 with LGM ^{14}C ventilation ages as low as 1400–1800 yr, except for a shelf ice-covered
769 site at the southern tip of Chile with IW ages of 2400–2900 yr, possibly a result of local
770 upwelling of CP waters. In general, however, the low values of Pacific IW are similar to
771 those estimated for South Atlantic IW and likewise reflect a vivid exchange with
772 atmospheric CO_2 in their source regions in the Southern Ocean (Skinner et al., 2015).
773
774 When entering and crossing the entrance sill to the marginal South China Sea the
775 'young' IW were mixed with 'old' CP waters entrained from below, here leading to ^{14}C
776 ventilation ages of 2600–3450 yr (Figs. 9 and S2d). The LGM South China Sea was
777 shaped by an estuarine-style overturning system marked by major upwelling near to its
778 distal end in the far southwest (Wang L. et al., 1999). This upwelling led to planktic ^{14}C
779 reservoir ages as high as 1200–1800 yr, values rarely found elsewhere in surface
780 waters of low latitudes.
781
782 Our wide-spaced distribution pattern of 18 open-ocean ^{14}C ventilation ages (plus 4
783 values based on paired wood chunks) in Figs. 10 and 11 agrees only in part with the
784 circulation patterns suggested by the much larger datasets of ^{14}C ventilation ages

785 compiled by Skinner et al. (2017) and Zhao et al. (2018). Several features in Figs. 10
786 and 11 directly deviate, e.g., the ages we derive for the North Atlantic and mid-depth
787 Pacific. These deviations may be linked to both the different derivation of our ^{14}C
788 ventilation age estimates and the details of our calendar-year chronology now based on
789 the narrow-standing suite of ^{14}C plateau-boundary ages. The quality of our ^{14}C reservoir
790 ages of surface waters also controls the 'apparent' ventilation age of deep-waters, as it
791 results from direct addition of the short-term average ^{14}C age of a planktic ^{14}C plateau to
792 a paired, that is coeval benthic ^{14}C age (formed during the time of benthic foraminiferal
793 growth, somewhat after the actual time of deep-water formation).
794
795 *3.3.2 — Major features of meridional overturning circulation during early HS-1 (Fig. 10)*
796
797 Near the onset of deglacial Heinrich Stadial 1 (HS-1; ~18–14.7 cal. ka) major shifts in
798 ^{14}C ventilation age suggest some short-lasting but fundamental changes in the
799 circulation geometry of the deep ocean, a central theme of marine paleoclimate
800 research (lower panel of Figs. 10, 11 and S2a and b). Deep waters in the eastern
801 Nordic Seas, west of the Azores Islands, and off northern Brazil show a rapid rise to
802 high ^{14}C ventilation ages of ~2000–2500 yr and up to 4000 yr off Brazil, values that give
803 first proof for a brief switch from ‘anti-estuarine’ to ‘estuarine’ circulation that governed
804 the central North Atlantic and Norwegian Sea during early HS-1. This geometry
805 continued – except for a brief but marked and widespread event of recurring NADW
806 formation near 15.2 ka – until the very end of HS-1 near 14.5 ka (Fig. S2a; Muschitiello
807 et al., 2019). The MOC switch from LGM to HS-1 is in line with changes depicted in
808 paired benthic $\delta^{13}C$ data (Sarnthein et al., 1994), but not confirmed by the coeval ε_{Nd}

809 record that suggests a constant source of 'mid-depth waters', with the $\delta^{13}C$ drop being
810 simply linked to a higher age (Howe et al., 2018).
811
812 Conversely, benthic ^{14}C ventilation ages in the northeastern North Pacific (Site MD02-
813 2489) show a coeval and distinct but brief minimum of 1050-1450 yr near 3640 m w.d.
814 during early HS-1 (~18.1–16.8 ka; Figs. 10, 11, and S2d). This minimum was produced
815 by extremely small benthic-planktic age differences of 350–650 yr and provides robust
816 evidence for a millennial-scale event of deep-water formation, that has flushed the
817 northeastern North Pacific down to more than 3640 m w.d. (Gebhardt et al., 2008;
818 Sarnthein et al., 2013; Rae et al., 2014). Similar circulation geometries were reported for
819 the Pliocene (Burls et al., 2017). 'Young' Upper North Pacific Deep Waters (North
820 Pacific Intermediate Waters *sensu* Gong et al., 2019) then penetrated as 'western
821 boundary current' far south, up to the northern continental margin of the South China
822 Sea (Figs. 9b, 11, and S2d). The short-lasting North Pacific regime of anti-estuarine
823 overturning was similar to that we find in the modern and LGM Atlantic and, most
824 interesting, simultaneous with the Atlantic's estuarine episode.
825
826 Recent data on benthic-planktic ^{14}C age differences (Du et al., 2018) precisely recover
827 our results in a core at ~680 m w.d. off southern Alaska. However, they do not depict
828 the 'young' deep waters at their Site U1418 at ~3680 m w.d., as corroborated by a
829 paired autigenic ε_{Nd} maximum suggesting a high local bottom water age nearby. We
830 assume that the amazing difference in local deep-water ventilation ages is due to small-
831 scale differences in the effect of Coriolis forcing at high latitudes between a site located
832 directly at the base of the Alaskan continental margin (U1418; Fig. 10b) and that on the
833 distal Murray Sea Mount in the 'open' Pacific (MD02-2489; Figs. 7 and 11), which

probably has been been washed by a plume of newly formed North Pacific deep waters probably stemming from the Bering and/or Ochotsk Seas. In contrast, the incursion of almost 3000 yr old deep waters from the Southern Ocean has continued along the continental margin all over HS-1. In summary we may conclude that the geometry of ocean MOC was briefly reversed in the 'open' North Pacific over almost 1500 years during HS-1, far deeper than suggested by previous authors (e.g., Okazaki et al., 2012; Gong, S., et al. 2019), but similar to changes in geometry first proposed by Broecker et al. (1985) then, however, for an LGM ocean.

3.3.3 — Deep-Ocean DIC inventory

Apart from the changing geometries in ocean MOC during LGM and HS-1, the global set of ^{14}C plateau-based, hence refined estimates of apparent ^{14}C ventilation ages (Fig. 10) has ultimately also revealed new insights into glacial-to-deglacial changes in deep-ocean DIC inventories (Sarnthein et al., 2013; Skinner et al., 2019). On the basis of GLODAP data (Key et al., 2004) any drop in ^{14}C concentration (i.e., any rise in average ^{14}C ventilation age) of modern deep waters is tied linearly to a rise of carbon (DIC) dissolved in deep ocean waters below ~2000 m, making for 1.22 micromole C / -1 ‰ ^{14}C. By and large, GCM and box model simulations of Chikamoto and Abé-Ouchi (2012) and Wallmann et al. (2016) suggest that this ratio may also apply to LGM deep-water circulation, when apparent ^{14}C ventilation ages in the Southern Ocean increased significantly (from 2400 up to ~3800 yr) and accordingly, thermohaline circulation was more sluggish and transit times of deep waters extended. Accordingly, a 'back-of-the-envelope' calculation of LGM ventilation age averages in the global deep ocean suggests an additional carbon absorption of 730–980 Gt (Sarnthein et al., 2013). This

859 estimate can easily accommodate the glacial transfer of ~200 Gt C from the atmosphere
860 and biosphere, moreover, may also explain 200–450 Gt C then most probably removed
861 from glacial Atlantic and Pacific intermediate waters. These estimates offer an
862 independent evaluation of ice core-based data, other proxies, and model-based data on
863 past changes in the global carbon cycle (e.g., Menviel et al., 2018).
864
865 4. SOME CONCLUSIONS AND PERSPECTIVES
866 – Despite some analytical scatter, ^{14}C ages for the top and base of Lake Suigetsu-
867 based atmospheric ^{14}C plateaus and coeval planktic ^{14}C plateaus do not present
868 statistical 'outliers' but real age estimates that are reproduced by tree ring-based ^{14}C
869 ages over the interval 10–13 cal. ka and further back.
870 – Hulu U/Th model-based ages of ^{14}C plateau boundaries of the Suigetsu atmospheric
871 ^{14}C record appear superior to those derived from microscopy-based varve counts only,
872 since U/Th model-based ages match far more closely the age when now deduced from
873 XRF-based varve counts for the tie point of lower plateau boundary 2b, a test case in
874 the early deglacial, and for the age assigned to the Laschamp event prior to the LGM.
875 – During deglacial times, we show that several atmospheric ^{14}C plateaus paralleled a
876 rise in air-sea gas exchange, and, in turn, distinct changes in ocean MOC. Changes in
877 cosmogenic ^{14}C production rarely provide a complete explanation for the plateaus
878 identified in the Suigetsu ^{14}C data under discussion.
879 – In total, ^{14}C plateau boundaries in the range now provide a suite of ~30 age tie points
880 to establish – like chronological ladder rungs – a robust global age control for deep-sea
881 sediment sections and global stratigraphic correlations of last glacial to deglacial climate
882 events, 29–10 cal. ka. U/Th model ages confine the cal. age uncertainty of Suigetsu
883 plateau boundaries assigned halfway between two ^{14}C ages nearby inside and outside

884 a plateau's scatter band to less than ±50 to ±70 yr. Nevertheless, stratigraphic gaps
885 may hamper the accurate tuning of planktic ^{14}C plateaus to their atmospheric
886 equivalents hence result in major discrepancies.
887 – The difference in ^{14}C age between coeval atmospheric and planktic ^{14}C plateaus
888 presents a robust tracer of planktic ^{14}C reservoir ages and shows their high temporal
889 and spatial variability for the LGM and HS-1, now established for 18/20 sediment sites.
890 – Paired reservoir ages obtained from different planktic species document the local
891 distribution patterns of different surface water masses and prevailing foraminiferal
892 habitats at different seasons yet insufficiently considered in model simulations.
893 – New, more robust deep-water ^{14}C ventilation ages, derived on the basis of our robust
894 planktic ^{14}C reservoir ages, reveal geometries of LGM overturning circulation similar to
895 those of today. In contrast, ^{14}C ventilation ages of early HS-1 suggest an almost 1500 yr
896 long event of widely reversed circulation patterns marked by deep-water formation and
897 brief flushing of the northern North Pacific and estuarine circulation geometry in the
898 northern North Atlantic.
899 – Increased glacial ^{14}C ventilation ages and carbon (DIC) inventories of ocean deep
900 waters suggest an LGM drawdown of about 850 Gt C into the deep ocean. Starting with
901 HS-1 a drop of ventilation age suggests carbon released to the atmosphere (Sarnthein
902 et al., 2013).
903 – Site-specific comparison of planktic and model-based reservoir ages estimates
904 highlights the need for further model refinements to make them better reflect the real
905 complex patterns of ocean circulation, including seasonality.
906

907 ACKNOWLEDGMENTS

We owe sincere thanks for plenty of stimulations to the 23rd International Radiocarbon Conference in Trondheim, in particular to M-J. Nadeau, and to the IPODS–OC3 workshop in Cambridge U.K, 2018, convened by A. Schmittner and L. Skinner. Moreover, we thank for most valuable basic discussions with R. Staff, Glasgow, J. Southon, Irvine CA, and M. Butzin, AWI Bremerhaven, who kindly helped us to discuss the comparison of his model results, and S. Beil, Kiel, for computer assistance. Over the last three years, G. Mollenhauer measured with care hundreds of supplementary ^{14}C ages in her MICADAS laboratory at AWI Bremerhaven. This study obtained long lasting special support from R. Tiedemann and his colleagues at the AWI Bremerhaven.

Author contribution

All authors contributed data and valuable suggestions to write up this synthesis. MS and PG designed the outline of this manuscript. KK, BA, TE and MS provided new marine ^{14}C records in addition to records previously published. GS displayed the details of Suigetsu varve counts. RM provided a ^{10}Be-based ^{14}C record and plots of raw ^{14}C data sets of Suigetsu und Hulu Cave. Discussions amongst PG, RM, GS and MS served to select U/Th-based model ages as best-possible time scale. JM streamlined the sections on data-model intercomparison.

Data availability

Published primary radiocarbon data of all sites are available at PANGAEA de. ^{14}C data of 5 marine cores still under publication by Küssner et al. (2020 subm.) and Ausin et al. (subm.; also see caption of Fig. S2) are deposited at PANGAEA.

REFERENCES (101)

Abé-Ouchi, A.: Deglaciation and DO-like experiments with MIROC AOGCM. Abstract, IPODS/OC3 -Workshop on 'Ocean circulation and carbon cycling during the last deglaciation: Global synthesis'. Cambridge 2018.

936 Adkins, J. F. and Boyle, E. A.: Changing atmospheric $\Delta^{14}C$ and the record of
937 paleoventilation ages. Paleoceanography, 12(3), 337–344, 1997.
938 Adolphi, F., Bronk Ramsey, C., Erhard, T., Lawrence Edwards, R., Cheng, H.,
939 Turney, C.S.M., Cooper, A., Svensson, A., Rasmussen, S.O., Fischer, H., and
940 Muscheler, R.: Connecting the Greenland ice-core and U/Th timescales via cosmogenic
941 radionuclides: testing the synchroneity of Dansgaard–Oeschger events. Clim. Past, 14,
942 1755–1781. https://doi.org/10.5194/cp-14-1755-2018, 2018.
943 Alves, E.Q., Macario, K., Ascough, P., and Bronk Ramsey, C.: The worldwide
944 marine radiocarbon reservoir effect: definitions, mechanisms, and prospects. Review of
945 Geophysics, 56, https://doi.org/10.1002/2017RG000588, 2018.
946 Alveson, E.Q.: Radiocarbon in the Ocean, EOS, 99,
947 https://doi.org/10.1029/2018EO095429, 2018.
948 Ausin, B., Haghipour, N., Wacker, L., Voelker, A. H. L., Hodell, D., Magill, C., et al.:
949 Radiocarbon age offsets between two surface dwelling planktonic foraminifera species
950 during abrupt climate events in the SW Iberian margin. Paleoceanography and
951 Paleoclimatology, 34. https://doi.org/10.1029/2018PA003490, 2019.
952 Ausin, B., Sarnthein, M., Haghipour, N., Lougheed, B., Wacker, L., and Eglinton,
953 T.J.: Glacial-to-deglacial radiocarbon history at the southwest Iberian margin.
954 Paleoceanography and Paleoclimate, 2020 subm.
955 Balmer, S., Sarnthein, M., Mudelsee, M., and Grootes, P. M.: Refined modeling and
956 ^{14}C plateau tuning reveal consistent patterns of glacial and deglacial ^{14}C reservoir ages
957 of surface waters in low-latitude Atlantic. Paleoceanography, 31.
958 https://doi.org/10.1002/2016PA002953, 2016.
959 Balmer, S. and Sarnthein, M.: Planktic ^{14}C plateaus, a result of short-term
960 sedimentation pulses? – Radiocarbon, 58, DOI:10.1017/RDC.2016.100, 11 pp., 2016.
961 Balmer, S. and Sarnthein, M.: Glacial-to deglacial changes in North Atlantic melt-
962 water advection and deep-water formation – Centennial-to-millennial-scale ^{14}C records
963 from the Azores Plateau. Geochim. Cosmochim. Acta, 236, 399-415,
964 https://doi.org/10.1016/j.gca.2018.03.001, 2018.
965 Berger W.H. and Keir, R.S.: Glacial-Holocene changes in atmospheric CO_2 and the
966 deep-sea record. J.E. Hansen, T. Takahashi (Eds.), Geophysical Monograph, 29,
967 American Geophysical Union, Washington, DC, pp. 337–351, 1984.
968 Bostock, H.C., Barrows, T.T., Carter, L., Chase, Z., Cortese, G., et al.: A review of
969 the Australian – New Zealand sector of the Southern Ocean over the last 30 ka (Aus-

970 INTIMATE project). Quaternary Science Reviews 74, 35-57, 2013.
971 Broecker W.S, Peteet, D.M., and Rind, D.: Does the ocean-atmosphere system have
972 more than one stable mode of operation? Nature, **315**, 21-26, doi:10.1038/315021a0,
973 1985
974 Broecker W.S., Barker, S., Clark, E., Hajdas, I., Bonani, G., and Stott, L.: Ventilation
975 of the Glacial deep Pacific Ocean, Science, 306, 1169–1172, 2004.
976 Bronk Ramsey, C., Staff, R. A., Bryant, C. L., Brock, F., Kitagawa, H., van der Plicht,
977 J., Schlolaut, G., Marshall, M. H., Brauer, A., Lamb, H. F., Payne, R. L., Tarasov, P. E.,
978 Haraguchi, T., Gotanda, K., Yonenobu, H., Yokoyama, Y., Tada, R., and Nakagawa, T.:
979 A complete terrestrial radiocarbon record for 11.2 to 52.8 kyr B.P., Science, 338, 370–
980 374, 2012.
981 Bronk Ramsey, C., Heaton, T.J., Schlolaut, G., Staff, R.A., Bryant, C.L., Lamb, H.F.,
982 Marshall, M.H., Nakagawa, T.: Reanalysis of the atmospheric radiocarbon calibration
983 record from Lake Suigetsu, Japan. Radiocarbon, https://doi.org/10.1017/RDC.2020.18,
984 2020
985 Burke, A. and Robinson, L.F.: The Southern Ocean's role in carbon exchange during
986 the last deglaciation. Science, 335, 557-561, 2012.
987 Burls, N.J., Fedorov, A.V., Sigman, D.M., Jaccard, S.L., Tiedemann, R., and Haug,
988 G.H.: Active Pacific meridional overturning circulation (PMOC) during the warm
989 Pliocene. Sci. Adv. 2017;3: e1700156, 2017.
990 Butzin, M., Prange, M., Lohmann, G.: Radiocarbon simulations for the glacial ocean:
991 The effects of wind stress, Southern Ocean sea ice and Heinrich events. Earth Planet.
992 Sci. Lett., 235, 45-61, 2005.
993 Butzin, M., Prange, M., and Lohmann, G.: Readjustment of glacial radiocarbon
994 chronologies by self-consistent three-dimensional ocean circulation modeling. Earth
995 Planet Sci. Lett., 317, 177-184, 2012.
996 Butzin, M., Köhler, P., and Lohmann, G.: Marine radiocarbon reservoir age
997 simulations for the past 50,000 years. Geophys. Res. Lett., 44, 8473–8480,
998 doi:10.1002/2017GL074688, 2017.
999 Butzin, M., Heaton, T.J., Köhler, P., and Lohmann, G.: A short note on marine
1000 reservoir age simulations used in INTCAL20. Radiocarbon, oo, 1-7, DOI:10.1017/RDC.2020.9,
1001 2020.
1002 Chen, T., Robinson, L.F., Burke, A., Southon, J., Spooner, P., Morris, P.J., and Ng,
1003 H.C.: Synchronous centennial abrupt events in the ocean and atmosphere during the

last deglaciation, Science, 349, 1537-1541, 2015.

Cheng, H., Edwards, R.L., Southon, J., Matsumoto, K., Feinberg, J.M., Sinha, A., Zhou, W., Li, H., Li, X., Xu, Y., Chen, S., Tan, M., Wang, Q., Wang, Y., and Ning, Y.: Atmospheric 14C/12C changes during the last glacial period from Hulu Cave, Science, 362, 1293-1297, 2018.

Chikamoto, M.O., Abé-Ouchi, A., Oka, A., Ohgaito, R., and Timmermann, A.: Quantifying the ocean's role in glacial CO_2 reductions, Climate of the Past, 8, 545–563, doi:10.5194/cp-8-545-2012, 2012.

Cook M.S. and Keigwin L.D.: Radiocarbon profiles of the NW Pacific from the LGM and deglaciation: Evaluating ventilation metrics and the effect of uncertain surface reservoir ages, Paleoceanography, 30, 174–195, 2015.

Davies, S.M., Davies, P.M., Abbott, Meara, R.H., et al.: A North Atlantic tephro-stratigraphical framework for 130-60 ka b2k: New tephra discoveries, marine based correlations, and future challenges, Quaternary Science Rev., 106, 101-121, 2014.

Du, J., Haley, B.A., Mix, A.C., Walczak, M.H., and Praetorius, S.K.: Flushing of the deep Pacific Ocean and the deglacial rise of atmospheric CO_2 concentrations, Nature geoscience, 11, 749-755, 2018.

Ferrari, R., Jansen, M.F., Adkins, J.F., Burke, A., Stewart, A.L., and Thompson, A.F.: Antarctic sea ice control on ocean circulation in present and glacial climates, Proc. National Academy Science, 111 (24), 8753–8758, 2014.

Gebbie, G.: How much did Glacial North Atlantic Water shoal? Paleoceanography, 29, 190-209, doi:10.1002/2013PA002557, 2014.

Gebhardt, H., Sarnthein, M., Kiefer, T., Erlenkeuser, H., Schmieder, F., and Röhl, U.: Paleonutrient and productivity records from the subarctic North Pacific for Pleistocene glacial terminations I to V. Paleoceanography 23, PA4212, 1-21, doi:10.1029/2007PA001513, 2008.

Gong, S., Lembke-Jene, L., Lohmann, G., Knorr, G., Tiedemann, R., Zou, J.J and Shi, X.F.: Enhanced North Pacific deep-ocean stratification by stronger intermediate water formation during Heinrich Stadial 1. Nature Communications, 10: 656. https://doi.org/10.1038/s41467-019-08606-2, 2019.

Grootes P.M. and Stuiver, M.: Oxygen 18/16 variability in Greenland snow and ice with 1000 to 100000 year time resolution, J. Geophys. Res.: Oceans (1978–2012) 102(C12), 26455–26470, 1997.

1037 Grootes, P.M. and Sarnthein, M.: Marine ^{14}C reservoir ages oscillate, PAGES News,
1038 14/3, 18-19, 2006.
1039 Hain, M.P., Sigman, D.M., and Haug, G.H.: Distinct roles of the Southern Ocean and
1040 North Atlantic in the deglacial atmospheric radiocarbon decline, Earth Planetary Science
1041 Letters 394, 198-208, 2014.
1042 Howe, J.N.W., Piotrowski, A.M., Noble, T.L., Mulitza, S., Chiessi, C.M., and Bayon,
1043 G.: North Atlantic deep-water production during the last glacial maximum, Nat.
1044 Commun., 7, 11765, 2016. s
1045 Howe, J.N.W., Huang, K-F., Oppo, D.W., Chiessi, C.M., Mulitza, S., Blusztajn, J.,
1046 and Piotrowski, A.M.: Similar mid-depth Atlantic water mass provenance during the Last
1047 Glacial Maximum and Heinrich Stadial 1, Earth Planetary Science Letters, 490, 51-61,
1048 2018.
1049 Jonkers, L. and Kucera, M.: Quantifying the effect of seasonal and vertical habitat
1050 tracking on planktonic foraminifera proxies, Climate of the Past, 13, 573-586, 2017.
1051 Keigwin, L.D. and Swift, S.A.: Carbon isotope evidence for a northern source of
1052 deep water in the glacial western North Atlantic, PNAS, 114 (11), 2831-2835, 2017.
1053 Key R. M., Kozyr, A., Sabine, C.L., Lee, K., Wanninkhof, R., Bullister, J.L., Feely,
1054 R.A., Millero, F.J., Mordy, C., and Peng, T.-H. (2004) A global ocean carbon climat-
1055 ology: Results from Global Data Analysis Project (GLODAP), Global Biogeochem. Cy.,
1056 18, GB4031, doi:10.1029/2004GB002247, 2004.
1057 Kong, X., Wang, Y., Wu, J., Cheng, H., Edwards, R.L., and Wang, X.: Complicated
1058 responses of stalagmite $\delta^{13}C$ to climate change during the last glaciation from Hulu
1059 Cave, Nanjing, China, Science in China Ser. D Earth Sciences, 48, (12), 2174-2181,
1060 2005.
1061 Küssner, K., Sarnthein, M., Lamy, F., and Tiedemann, R.: High-resolution
1062 radiocarbon-based age records trace episodes of *Zoophycos* burrowing, Marine
1063 Geology, 403, 48-56, http://doi:10.1016/j.margeo.2018.04.01, 2018.
1064 Küssner, K., Sarnthein, M., Lamy, F., Michel, E., Mollenhauer, G., Siani G., and
1065 Tiedemann, R.: Glacial-to-deglacial reservoir ages of surface waters in the southern
1066 South Pacific. Paleoceanography and Paleoclimate, 54 ms-pp, 2020 subm.
1067 Lascu, I., Feinberg, J.M., Dorale, J.A., Cheng, H., and Edwards, R.L.: Age of the
1068 Laschamp excursion determined by U-Th dating of a spelothem geomagnetic record
1069 from North America. Geology, 44, 139-142, doi:10.1130/G37490.1. 2016

1070 Lindsay, C.M., Lehman, S.J., Marchitto, T.M., and Ortiz, J.D.: The surface
1071 expression of radiocarbon anomalies near Baja California during deglaciation. Earth
1072 Planetary Science Letters, 422, 67-74, 2015.
1073 Lippold, J., Gutjahr, M., Blaser, P., Christner, E., de Cavalho-Fereira, M.L., Mulitza,
1074 S. et al.: Deep-water provenance and dynamics of the (de)glacial Atlantic meridional
1075 overturning circulation, Earth Planetary Science Letters, 445, 68-78, 2016.
1076 Lisiecki, L.E. and Stern, J.V.: Regional and global benthic $d^{18}O$ stacks for the last
1077 glacial cycle. Paleoceanography, 31, doi:10.1002/2016PA003002, 2016.
1078 Löwemark, L. and Grootes, P.M.: Large age differences between planktic
1079 foraminifers caused by abundance variations and Zoophycos bioturbation,
1080 Paleoceanography, 19, PA2001, doi:10.1029/2003PA000949, 2004.
1081 Marcott, S.A., Bauska, T.K., Buizert, C., Steig, E.J., Rosen, J.L., Cuffey, K.M.,
1082 Fudge, T.J., Severinghaus, J.P., Ahn, J., Kalk, M.L., McConnell, J.R., Sowers, T.,
1083 Taylor, K.C., White, J.W.C., and Brook, E.J.: Centennial-scale changes in the global
1084 carbon cycle during the last deglaciation, Nature, 514, 616-619,
1085 doi:10.1038/nature13799, 2014.
1086 Marshall, M., Schlolaut, G., Brauer, A., Nakagawa, T., Staff, R.A., Bronk Ramsey,
1087 C., Lamb, H., Gotanda, K., Haraguchi, T., Yokoyama, Y., Yonenobu, H., Tada, R.,
1088 SG06 project members: A novel approach to varve counting using μXRF and X-
1089 radiography in combination with thin-section microscopy, applied to the Late Glacial
1090 chronology from Lake Suigetsu, Japan, Quaternary Geochronology 13, 70-80, 2012.
1091 McCave, I.N., Carter, I., and Hall, I.R.: Glacial-interglacial changes in water mass
1092 structure and flow in the SW Pacific Ocean, Quaternary Science Rev., 27, 1886–1908,
1093 2008.
1094 Matsumoto, K.: Radiocarbon-based circulation age of the world oceans, J. Geophys.
1095 Res.: Oceans 112(C9), C09004. https://doi.org/10.1029/2007JC004095, 2007.
1096 Menviel, L., Spence, P., Yu, J., Chamberlain, M.A., Matear, R.J., Meissner K.J., and
1097 England, M.H.: Southern Hemisphere westerlies as a driver of the early deglacial
1098 atmospheric CO2 rise, Nature communications, 9:2503, DOI:10.1038/s41467-018-
1099 04876-4, 2018.
1100 Millo, C., Sarnthein, M., and Erlenkeuser, M.: Variability of the Denmark Strait
1101 Overflow during the Last Glacial Maximum, Boreas, 35, 50-60, 2006.
1102 Muglia, J., Skinner, L., and Schmittner, A.: Weak overturning circulation and high
1103 Southern Ocean nutrient utilization maximized glacial ocean carbon, Earth and

Planetary Science Letters 496, 47-56, 2018.

Muschitiello, F., D'Andrea, W.J., Schmittner, A., Heaton, T.J., Balascio, N.L., deRoberts, N., Caffee, M.W., Woodruff, T.E., Welten, K.C., Skinner, L.C., Simon, M.H., and Dokken T.M.: Deep-water circulation changes lead North Atlantic climate during deglaciation, Nature Communications 10, 1272, doi.org/10.1038/s41467-019-09237-3, 2019.

Naughton, F., Costas, S., Gomes, S.D., Desprat, S., Rodrigues, T., Sanchez Goñi, M.F., Renssen, H., Trigo, R., Bronk-Ramsey, C., Oliveira, D., Salgueiro, E., Voelker, A.H.L., and Abrantes, F.: Coupled ocean and atmospheric changes during Greenland stadial 1 in southwestern Europe, Quaternary Science Reviews, 212, 108-120, 2019.

Nydal R., Lovseth K., and Skogseth F. H.: Transfer of bomb ^{14}C to the ocean surface, Radiocarbon 22(3), 626–635, 1980.

Okazaki, Y., Sagawa, T., Asahi, H., Horikawa, K., and Onodera, J.: Ventilation changes in the western North Pacific since the last glacial period, Climate of the Past, 8, 17-24, doi:10.5194/cp-8-17-2012, 2012.

Paillard, D., Labeyrie, L., and Yiou, P.: Macintosh program performs time-series analysis, *Eos Trans, AGU,* **77**: 379, 1996.

Rae, JW.B. and W. Broecker, W.: What fraction of the Pacific and Indian oceans' deep water is formed in the Southern Ocean? Biogeosciences, 15, 3779-3794, 2018.

Rae, J., Sarnthein, M., Foster, G., Ridgwell, A., Grootes, P.M., and Elliott T.: Deep water formation in the North Pacific and deglacial CO_2 rise*,* Paleoceanography, 29, doi:10.1002/2013PA002570, 645–667, 2014.

Rafter, P.A., Herguera, J.-C., and Southon, J.R.: Extreme lowering of deglacial seawater radiocarbon recorded by both epifaunal and infaunal benthic foraminifera in a wood-dated sediment core, Climate of the Past 14, 1977–1989, 2018.

Reimer P.J., Bard, E., Bayliss, A., Beck, J. W., Blackwell, P.G., Bronk Ramsey, C., Buck, C.E., Cheng, H., Edwards, R.L., and Friedrich, M.: IntCal13 and Marine13 radiocarbon age calibration curves 0–50,000 years cal. BP, Radiocarbon 55, 1869–1887, 2013.

Reimer, P.J., et al.: The IntCal 20 northern hemisphere radiocarbon calibration curve (0-55 kcal BP), Radiocarbon, 2020 (in press).

Robinson, L.F., Adkins, J.F., Keigwin, L.D., et al..: Radiocarbon variability in the western North Atlantic during the last deglaciation, Science, 310, 1469-1473, 2005.

1137 Ronge, T. A., Tiedemann, R., Lamy, F., et al.: Radiocarbon constraints on the extent
1138 and evolution of the South Pacific glacial carbon pool, Nature Comm. 7:11487, 2016.
1139 Ronge, T.A., Sarnthein, M., Roberts, J., Lamy, F., and Tiedemann, R.: East Pacific
1140 Core PS75/059-2: Glacial-to-deglacial stratigraphy revisited, Paleoceanography and
1141 Paleoclimatology, 34 (4), 432-435, DOI:10.1029/2019PA003569, 2019.
1142 Sarnthein, M., Winn, K., Jung, S.J., Duplessy, J.C., Labeyrie, L., Erlenkeuser, H.,
1143 and Ganssen, G.: Changes in east Atlantic deepwater circulation over the last 30,000
1144 years: eight time slice reconstructions, Paleoceanography, 9(2), 209–267, 1994.
1145 Sarnthein, M., Pflaumann, U., and Weinelt, M.: Past extent of sea ice in the northern
1146 North Atlantic inferred from foraminiferal paleotemperature estimates,
1147 Paleoceanography, 18(2), 2003.
1148 Sarnthein, M., Grootes, P.M., Kennett, J.P., and Nadeau, M.: ^{14}C Reservoir ages
1149 show deglacial changes in ocean currents and carbon cycle, Geophys. Monograph –
1150 Am. Geophys. Union, 173, 175–196, 2007.
1151 Sarnthein, M., Grootes, P.M., Holbourn, A., Kuhnt, W., and Kühn, H.: Tropical
1152 warming in the Timor Sea led deglacial Antarctic warming and almost coeval
1153 atmospheric CO_2 rise by >500 yr, Earth Planetary Science Letters, 302, 337-348, 2011.
1154 Sarnthein, M., Schneider, B., and Grootes, P.M.: Peak glacial 14C ventilation ages
1155 suggest major draw-down of carbon into the abyssal ocean, Climate of the Past, 9 (1),
1156 925–965, 2013.
1157 Sarnthein, M., Balmer, S., Grootes, P.M., and Mudelsee, M.: Planktic and benthic
1158 14C reservoir ages for three ocean basins, calibrated by a suite of 14C plateaus in the
1159 glacial-to-deglacial Suigetsu atmospheric 14C record, Radiocarbon, 57, 129–151, 2015.
1160 Sarnthein, M. and Werner, K.: Early Holocene planktic foraminifers record species-
1161 specific ^{14}C reservoir ages in Arctic Gateway, Marine Micropaleontology, 135, 45-55.
1162 DOI:10.1016/j.marmicro.2017.07.002, 2018.
1163 Schlolaut, G.: A unique and easy-to-use-tool to deal with incompletely varved
1164 archives 782 – the Varve Interpolation Program 3.0.0, Quaternary Geochronology, 2019
1165 (in press).
1166 Schlolaut, G., Staff, R.A., Marshall, M.H., Brauer, A., Bronk Ramsey, C., Lamb, H.F.,
1167 and Nakagawa, T.: Microfacies analysis of the Lake Suigetsu (Japan) sediments from
1168 ~50 to ~10 ka BP and an extended and revised varve based chronology, Quaternary
1169 Science Reviews, 200, 351-366, 2018.

1170 Schmittner, A. and Lund, D.C.: Early deglacial Atlantic overturning decline and its
1171 role in atmospheric CO_2 rise inferred from carbon isotopes ($\delta^{13}C$), Climate of the Past,
1172 11, 135-152, 2015.
1173 Schroeder, J., Holbourn, A., Küssner, K., and Kuhnt, W.: Hydrological variability in
1174 the southern Makassar Strait during the last glacial termination, Quaternary Science
1175 Reviews, 154, 143-156, 2016.
1176 Sessford, E.G., Jensen, M.F., Tisserand, A.A., Muschitiello, F., Dokken, T.,
1177 Nisancioglu, K.H., and Jansen, E.: Consistent fluctuations on intermediate water
1178 temperature off the coast off Greenland and Norway suring Dansgaard-Oeschger
1179 events, Quaternary Science Reviews, 223, 105887, 1-17, 2019.
1180 Sherriff-Tadano, S., Abe-Ouchi, A., Yoshimori, M., Oka, A., and Chan, W.-L.:
1181 (Influence of glacial ice sheets on the Atlantic meridional overturning circulation through
1182 surface wind change, Climate Dynamics, 50 (7-8), 2881–2903, 2017.
1183 Siani, G., Michel, E., De Pol-Holz, R., DeVries, T., Lamy, F., Carel, M., Isguder, G.,
1184 Dewilde, F., Lourantou, A.: Carbon isotope records reveal precise timing of enhanced
1185 Southern Ocean upwelling during the last deglaciation, Nature Communications, 4,
1186 2758, 2013.
1187 Sikes, E.L. and Guilderson, T.P.: Southwest Pacific Ocean surface reservoir ages
1188 since the last deglaciation: Circulation insights from multiple-core studies. Paleocean-
1189 ography, 31, 298–310, doi:10.1002/2015PA002855, 2016.
1190 Simstich, J., Sarnthein, M., and Erlenkeuser, H.: Paired $\delta^{18}O$ signals of
1191 *Neogloboquadrina pachyderma* (s) and *Turborotalita quinqueloba* show thermal
1192 stratification structure in Nordic Seas, Mar. Micropaleontol., 912, 1–19, 2003.
1193 Skinner, L.C., Fallon, S., Waelbroeck, C., Michel, E., and Barker, S.: Ventilation of
1194 the deep Southern Ocean and deglacial CO2 rise, Science, 328, 1147–1151, 2010.
1195 Skinner, L.C., Waelbroeck, C., Scrivner, A.E., and Fallon, S.J.:Radiocarbon
1196 evidence for alternating northern and southern sources of ventilation of the deep
1197 Atlantic carbon pool during the last deglaciation, PNAS, 111, 5480–5484, 2014.
1198 Skinner, L.C. *et al.*: Reduced ventilation and enhanced magnitude of the deep
1199 Pacific carbon pool during the last glacial period, Earth Planetary Science Letters, **411**,
1200 45-52, 2015.
1201 Skinner, L.C., Primeau, F., Freeman, E., de la Fuente, M., Goodwin, P.A.,
1202 Gottschalk, J., Huang, E., McCave, I.N., Noble, T.L., and Scrivner A.E.: Radiocarbon

constraints on the glacial ocean circulation and its impact on atmospheric CO_2, Nature communications, 8:16010, DOI: 10.1038/ncomms16010, 2017.

Skinner, L.C., Muschitiello, F., and Scrivner, A.E.: Marine reservoir age variability over the last deglaciation: Implications for marine carbon cycling and prospects for regional radiocarbon calibrations. Paleoceanography and Paleoclimate, 34, doi.org/10.1029/2019PA003667, 2019.

Southon, J., Noronha, A.L., Cheng, H, Edwards, R.L., and Wang, Y.: A high-resolution record of atmospheric ^{14}C based on Hulu Cave speleothem H82, Quaternary Science Reviews, 33:32-41, 2012.

Steffensen, J.P., Andersen, K.K., Bigler, M., et al.: High-Resolution Greenland Ice Core Data Show Abrupt Climate Change Happens in Few Years, Science, 321, 680; DOI: 10.1126/science.1157707, 2008.

Stern, J.V. and Lisiecki, L.E.: North Atlantic circulaton and reservoir age changes over the past 41,000 years, Geophysical Research Letters, 40, 3693-3697, doi:10.1002/grl.5067, 2013.

Stocker, T. and Johnsen, S.J.: A minimum thermodynamic model for the bipolar seesaw, Paleoceanography, 18 (4), 1087, doi:10.1029/2003PA000920, 2003.

Stuiver, M. and Braziunas, T.V.: Modeling atmospheric ^{14}C influences and ^{14}C ages of marine samples to 10,000 B.C., Radiocarbon, 35, 137–189, 1993.

Svensson, A., Andersen, K.K., Bigler, M., Clausen, H.B., Dahl-Jensen, D., Davies, S.M., Johnsen, S.J., Muscheler, R., Parrenin, F., Rasmussen, S.O., Röthlisberger, R., Seierstad, I., Steffensen, J.P., and Vinther, B.M.: A 60 000 year Greenland stratigraphic ice core chronology, Climate of the Past, 4, 47–57, 2008.

Toggweiler, J.R., Druffel, E.R.M., Key, R.M., and Galbraith, E.D.: Upwelling in the ocean basins north of the ACC. Part 2: How cool Subantarctic water reaches the surface in the tropics, J. Geophysical Research, DOI:10.1029/2018JC014795, 2019 (in press).

Turney, C.S.M., Fifield, L.K., Hogg, A.G., et al.: Using New Zealand kauri (*Agathis australis*) to test the synchronicity of abrupt climate change during the Last Glacial Interval (60,000–11,700 years ago), Quatern. Sci. Rev., 29, 3677–3682, 2010.

Turney, C.S.M., Jones, R.T., Phipps, S.J., et al.: Rapid global ocean-atmosphere response to Southern Ocean freshening during the last glacial, Nature communications, 8:520, doi:10.1038/s41467-017-00577-6, 2017.

Umling, N.E. and Thunnell, R.C.: Synchronous deglacial thermocline and deep-water ventilation in the eastern equatorial Pacific, Nature communications, 8, 14203. DOI: 10.1038/ncomms14203, 2017.

Waelbroeck, C., Duplessy, J.-C., Michel, E., Labeyrie, L., Paillard, D., and Duprat, J.: The timing of the last deglaciation in North Atlantic climate records, Nature, 412, 724–727, 2001.

Waelbroeck, C., Skinner, L.C., Labeyrie, L., Duplessy, J.-C., Michel, E., Riveiros, N.V., Gherardi, J.-M., and Dewilde, F.: The timing of deglacial circulation changes in the Atlantic, Paleoceanography, 26, PA3213, https://doi.org/10.1029/2010PA002007, 2011.

Wallmann, K., Schneider, B., and Sarnthein, M.: Effects of eustatic sea-level change, ocean dynamics, and nutrient utilization on atmospheric pCO_2 and seawater composition over the last 130,000 years – a model study, Climate of the Past, 12, 339-375, doi: 10.5194/cp-12-339-2016, 2016.

Wang Y.C, Cheng, H., Edwards, R.L., An, Z.S., Wu, J.Y., Shen, C.-C., and Dorale, J.A.: A high-resolution absolute-dated Late Pleistocene monsoon record from Hulu Cave, China, Science, 294, 2345-2348. DOI: 10.1126/science.1064618, 2001.

Wang, L.J., Sarnthein, M., Erlenkeuser, H., Grimalt, J., Grootes, P., Heilig, S., Ivanova, E., Kienast, M., Pelejero, C., and Pflaumann, U.: East Asian monsoon climate during the late Pleistocene: High-resolution sediment records from the South China Sea, Marine Geology, 156, 245-284, 1999.

Wang, P., Clemens, S., Beaufort, L., Braconnot, P., Ganssen, G., Jian, Z., Kershaw, P., and Sarnthein, M.: SCOR/IMAGES Working Group 113 SEAMONS: Evolution and variability of the Asian Monsoon System: State of the art and outstanding issues, Quaternary Science Reviews, 24 (5-6), 595-629, 2005.

WAIS Divide Project Members: Onset of deglacial warming in West Antarctica driven by local orbital forcing. Nature, 500, 440-444. doi:10.1038/nature12376, 2013.

Xu, J., Kuhnt, W., Holbourn, A., Regenberg, M., and Andersen, N.: Indo-Pacific Warm Pool variability during the Holocene and Last Glacial Maximum, Paleoceanogr., 25, 16, 2010.

Yamamoto, A., Abe-Ouchi, A., Ohgaito, R., Ito, A., and Oka, A.: Glacial CO_2 decrease and deep-water deoxygenation by iron fertilization from glaciogenic dust, Climate of the Past, 15, 981-996.

Yashayaev, I., Seidov, D., and Demirov, E.: A new collective view of oceanography of the Arctic and North Atlantic basins, Progress in Oceanography, 132, 21 pp.,

DOI:http://dx.doi.org/10.1016/j.pocean.2014.12.012, 2015.

Zhao, N. and Keigwin, L.D.: An atmospheric chronology for the glacial-deglacial Eastern Equatorial Pacific, Nature communications, 9:3077, DOI:10.1038/s41467-018-05574-x, 2018.

Zhao, N., Marchal, O., Keigwin, L., Amrhein, D., and Gebbie, G.: A synthesis of deep-sea radiocarbon records and their (in) consistency with modern ocean ventilation, Paleoceanography and Paleoclimatology, 33, 128-151, 2018.

TABLE CAPTIONS

Table 1 a and b. Summary of varve- and U/Th model-based age estimates (Schlolaut et al., 2018; Bronk Ramsey et al., 2012) for ~30 plateau (pl.) boundaries in the atmospheric ^{14}C record identified in Lake Suigetsu Core $SG06_{2012}$ by means of visual inspection over the interval 10.5–27 cal. ka (Sarnthein et al., 2015, suppl. and modified). At the right hand side, three columns give the average (Ø) and uncertainty range of ^{14}C ages for each ^{14}C plateau.

SUIGETSU SG06_2012 Plateau no.	Plateau Top **Varve-based** age (yr BP)	***U/Th-based*** *age (yr BP)*	Depth (cm c.d.)	Plateau Base **Varve-based** age (yr BP)	***U/Th-based*** *age (yr BP)*	Depth (cm c.d.)	Ø 14C Age of 14C Plateau (14C yr)	±Uncertainty (14C yr)	14C age BP min/max. (1.6 σ range)
'Preboreal'	10525	***10560***	1325	11100	***11108***	1383	**9525**	–170/+110	9356/ 9635
'Top YD'	11290	***11281***	1402	11760	***11755***	1453	**10060**	–100/+35	9963/ 10095
'YD'	11950	***11895***	1467	12490	***12475***	1525	**10380**	–170/ 124	10211/ 10504
'no name'	12885	***12780***	1555	13160	***13080***	1582	**11000**	–85/ 114	10915/ 11114
1a	13580	***13656***	1626	13980	***14042***	1657	**12006**	100	11857/ 12050
1	14095	***14160***	1666	15095	***15100***	1740	**12471**	185	12315/ 12683
2a	15310	***15420***	1754	16140	***16520***	1802	**13406**	245	13174/ 13665
2b	16075	***16520***	1802	16400	***16930***	1820	**13850**	40	13808/ 13885
3	16835	***17500***	1847	17500	***18220***	1888	**14671**	105	14582/ 14792
4	17880	***18650***	1913	18830	***19590***	1971	**15851**	190	15661/ 16044

5a	18960	***19720***	1978	19305	***20240***	2003	**16670**	90	16570/ 16750
5b	19305	***20240***	2003	20000	***20900***	2032	**17007**	190	16830/ 17247
6a	20190	***21000***	2050	20920	***21890***	2105	**17667**	262	17435/ 17960
6b	20920	***21890***	2105	21275	***22300***	2132	**18075**	140	17960/ 18240
7	21375	***22400***	2140	21790	***22870***	2171	**18843**	117	18741/ 18975
8	21835	***22940***	2175	22730	***24250***	2257	**19715**	–290 325	19425/ 20041
9	22730	***24250***	2257	23395	***25150***	2312	**20465**	–227 263	20238/ 20728
10a	23935	***25880***	2358	25080	***27000***	2400	**22328**	–380 270	21946/ 22600
10b	25080	***27000***	2400	25800	***27600***	2426	**22708**	–475 440	22233/ 23147
11	26110	***27770***	2443	27265	***28730***	2525	**24088**	–360 505	23727/ 24595

1286

1287

~~V~~ **Table 2**. Temporal match of various ^{14}C plateaus with deglacial periods of major atmospheric CO_2 rise and ocean warmings (AA = Antarctic; GIS = Greenland Interstadial).

pCO_2 RISE (~12 ppm) AGE based on annual layers AA ice core (Marcott et al. 2014)	Plateau no.	Plateau boundaries AGE range (cal. ka) based on **U/Th model ages** (Bronk Ramsey et al., 2012)
11.7 – 11.5	# 'Top YD'	**11.83 – 11.3**
14.8 – 14.53	# 1	**15.1 – 14.2**
16.4 – 16.15	# 2a	**16.52 – 15.5**
17.4 – ~17.1	(data gap)	**17.3 – 17.1**

FURTHER POTENTIAL CORRELATIVES:

Progressive N. Atlantic warming during the YD at 12.39 – 12.03 ka *	# 'YD'	**12.46 – 11.98**
Onset of Antarctic ** warming at 18.3–17.6 ka (ice-based time scale)	#3	**18.22 – 17.5**
Onset of North Atlantic *** warming at 19.3–18.6 ka (U/Th-based time scale)	# 4	**19.6 – 18.65**
Top H2: GIS 2 N. Atlantic warming at 23.4 – 23.3 ka ****	#8	**24.25 – 22.95**

AGE CONTROL based on

* Naughton et al. (2019), ** Kawamura et al. (2007),

*** Balmer and Sarnthein (2018), **** Grootes and Stuiver (1997)

~~V~~ **Table 3** a-c. ^{14}C reservoir / ventilation ages of surface (top 50-100 m) and bottom waters vs. U/Th-based model age at 19/22 core sites in the ocean. (a) Spatial and temporal changes over early and late LGM (24–21 and 21–18.7 cal. ka), (b) HS-1, and the B/A. Late LGM estimates (average res. age of Plateau 4-5) are compared to model-based estimates of Muglia et al. (2018). (c) Data sources. For core locations see Fig. 7.

(a)

Sediment Core U/Th-based model age Plateau (Pl.) no.	Latitude	Longitude	Water depth (m)	LGM pla. res. age 24–21 ka (early LGM) Pl. 8 - 7 - 6	 Error (yr)	 21–18.7 ka (late LGM) Pl. 5 - 4	 Error (yr)	LGM model strong AMOC (yr)	res. age weak (yr)
ATLANTIC O.									
PS2644	67°52.02'N	21°45.92'W	777	2100	±390	1920–2200	±325 –±12	1136	1100
GIK 23074	66°66.67'N	4°90'E	1157	620–790	±145–±270	550–1175	±100–±200	1054	1059
MD08-3180	38°N	31°13.45'W	3064	–		320–605	±125–±405	827	887
SHAK06-5K	37°34'N	10°09'W	2646	675–800		500–660		872	855
(= MD99-2334)	(37°48'N	10°10'W	3146						
ODP 1002	10°42.37'N	65°10.18'W	893	700–210	±230–±310	25 – -205	±205–±215	751	738
GeoB 3910-1	4°15'S	36°21'W	2361	–		–		779	796
GeoB 1711-4	23°17'S	12°23'W	1976	1080	±290	730–840	±240–±190	711	721
KNR 159-5-36GGC	27°31'S	46°48'W	1268	540	±140	870	±120	757	777
MD07-3076	44°4'S	4°12'W	3770	–		2300	±200	928	989
INDIAN O./TIMOR SEA									
MD01-2378	13°08.25'S	121°78.8'E	1783	–		2000–1700	±300–±320	885	890
PACIFIC O.									
MD02-2489	54°39.07'N	148°92.13'W	3640	–		1560–1110	±310–±335	972	965
MD01-2416	51°26.8'N	167°72.5'E	2317	–		1710	±440	1227	1202
ODP 893A	34°17.25'N	120°02.33'W	588	–		1065	±280	839	846
MD02-2503	34°16.6'N	120°01.6'W	580	–		–		839	846
GIK 17940	20°07.0'N	117°23.0'E	1727	1820–1260	±320–±230	hiatus		836	838
(= SO50-37)	18°55'N	115°55'E	2655	1820–1260				836	840
PS75/104-1	44°46'S	174°31'E,	835	1650–1280	±210-±320	1500	±340	881	895
(= SO213-84)	45°7.5'S	174°34,9'E	972	1650–1280	±210-±320	1500	±340	881	895
MD07-3088	46°S	75°W	1536	385	±315	380-450	±140–±230	917	–
SO213-76-2	46°13'S	178°1.7´W	4339	–		1460–990	±340–±550	915	842
PS97/137-1	52°39.5'S	75°33.9'E	1027	600–1180	±465	1180–800	±90–±225	1505	1419

1299 (b)

Sediment Core	HS-1 pla. res. age				B/A pla. res. age		LGM be. vent age		LGM b.w. model age	
U/Th-based model a	18 –16.5 ka		16.5–15.5 ka		14.7 –13.6 ka		(yr)		strong AMOC	weak
Plateau (Pl.) no.	Pl. 3 - 2b (yr)	Error (yr)	Pl. 2a (yr)	Error (yr	Pl. 1 - 1a	Error (yr)	early	late	(yr)	(yr)
ATLANTIC O.										
PS2644	1775–1660	±105–±16(	1900	±355	–		345	2400	948	918
GIK 23074	1730–2000	±125–±16(	670	±310	140–310	±250–±10(	375	375	960	931
MD08-3180	1420–1610	±310–±16(	1460	±390	630–360	±310	600	600	1031	1004
SHAK06-5K	330–410		535		780–925		—		—	—
(= MD99-2334)							2200–2700	1900	—	—
ODP 1002	–100 – 20	±140	90	±345	355	±200	—		1247	1175
GeoB 3910-1	630–560	±160–±18(	175	±475	210–230	±220–±11(	2150	2150	—	—
GeoB 1711-4	660–690	±195–±45	420	±320	880	±255	1500	1500	1387	1714
KNR 159-5-36GGC	460–340	±380–±30(	170	±700	180–230	±370–±31(	1470	1470	1354	1563
MD07-3076	1650	±180	–		920	±230	3640	3640	1653	2060
INDIAN O./TIMOR SEA										
MD01-2378	740	±125	–		200–185	±345–±13	2720	—	1679	1881
PACIFIC O.										
MD02-2489	800–550	±155–±12(	550	±305	440	±285		2625	2332	2595
MD01-2416	1480–1140	±135–±19	–		720–570	±285–±140		3700/5100	2400	2683
ODP 893A	1065–1490	±280–±12	1400	±370	520	±185		1430	1677	1705
MD02-2503	965–1365	±160–±16	1215	±325	395–535	±240–±13(	—	—	—	—
GIK 17940	1210–1370	±200–±47(	1045	±320	870–970	±325–±10(	3300–1800		1807	1897
(= SO50-37)							3225	3225	2373	2667
PS75/104-1	1050	±265	1180	±350	800	±280	—	—	—	—
(= SO213-84)							1500	2400	1101	1146
MD07-3088	800–1090	±85–±125	1060	±275	1310–730	±125–±19(	1360 ?	1600	1808	1701
SO213-76-2	840	±310	–		–			3460	1712	2001
PS97/137-1	1500–670	±90–±180	455	±270	–		1400–2400	2400/2900	1631	1871

1300

1301 (c)

Sediment Core	DATA Source	
ATLANTIC O.		
PS2644	Sarnthein et al. 2015	Be.data suppl.
GIK 23074	Sarnthein et al. 2015	Be.data suppl.
MD08-3180	Balmer et al. 2018	
SHAK06-5K	Ausin et al., 2020 subm.	
(= MD99-2334)	Skinner et al. 2014	
ODP 1002	Sarnthein et al. 2015	
GeoB 3910-1	Balmer et al. 2016	
GeoB 1711-4	Balmer et al. 2016	
KNR 159-5-36GGC	Balmer et al. 2016	data suppl.
MD07-3076	Balmer et al. 2016	
INDIAN O./TIMOR SEA		
MD01-2378	Sarnthein et al. 2015	
PACIFIC O.		
MD02-2489	Sarnthein et al. 2015	
MD01-2416	Sarnthein et al. 2015	modified
ODP 893A	Sarnthein et al. 2015	data suppl.
MD02-2503	Sarnthein et al. 2015	
GIK 17940	Sarnthein et al. 2015	
(= SO50-37)	Sarnthein et al. 2015	
PS75/104-1	Küssner et al., 2018+2020	
(= SO213-84)	Ronge et al., 2016	
MD07-3088	Küssner et al.,2020 subm	Siani et al. 2013
SO213-76-2	Küssner et al.,2020 subm	Ronge et al.2016
PS97/137-1	Küssner et al.,2020 subm	data suppl.

1302 (c)

FIGURE CAPTIONS

– Fig. 1. Atmospheric ^{14}C ages of Lake Suigetsu plant macrofossils 10–20 cal. ka (bottom panel) and 19–29 cal. ka (top panel) vs. U/Th-based model age (blue dots; Bronk Ramsey et al., 2012). The 1:1 line reflects gradient of one ^{14}C yr / cal. yr. Double and triple ^{14}C measurements are averaged. (In part large) error bars of single ^{14}C ages are given in Suppl. Fig. S1. Suite of labeled horizontal boxes that envelop scatter bands of largely constant ^{14}C ages shows ^{14}C plateaus longer than 250 yr (plateau boundary ages listed in Table 1). Red and brown dots (powder samples from trench and wall) and + signs (off-axis samples) depict raw ^{14}C ages of Hulu stalagmites H82 and MSD (Cheng et al., 2018; Southon et al., 2012; plot offset by +3000 ^{14}C yr). Suite of short ^{14}C plateaus (black boxes) tentatively assigned to Hulu-based record occupies age ranges slightly different from those deduced for Suigetsu-based plateaus. The difference possibly results from short-term changes in the Old / Dead Carbon Fraction (ocf / dcf) that in turn may reflect major short-term changes in LGM and deglacial monsoon climate (Wang et al., 2001; Kong et al., 2005).

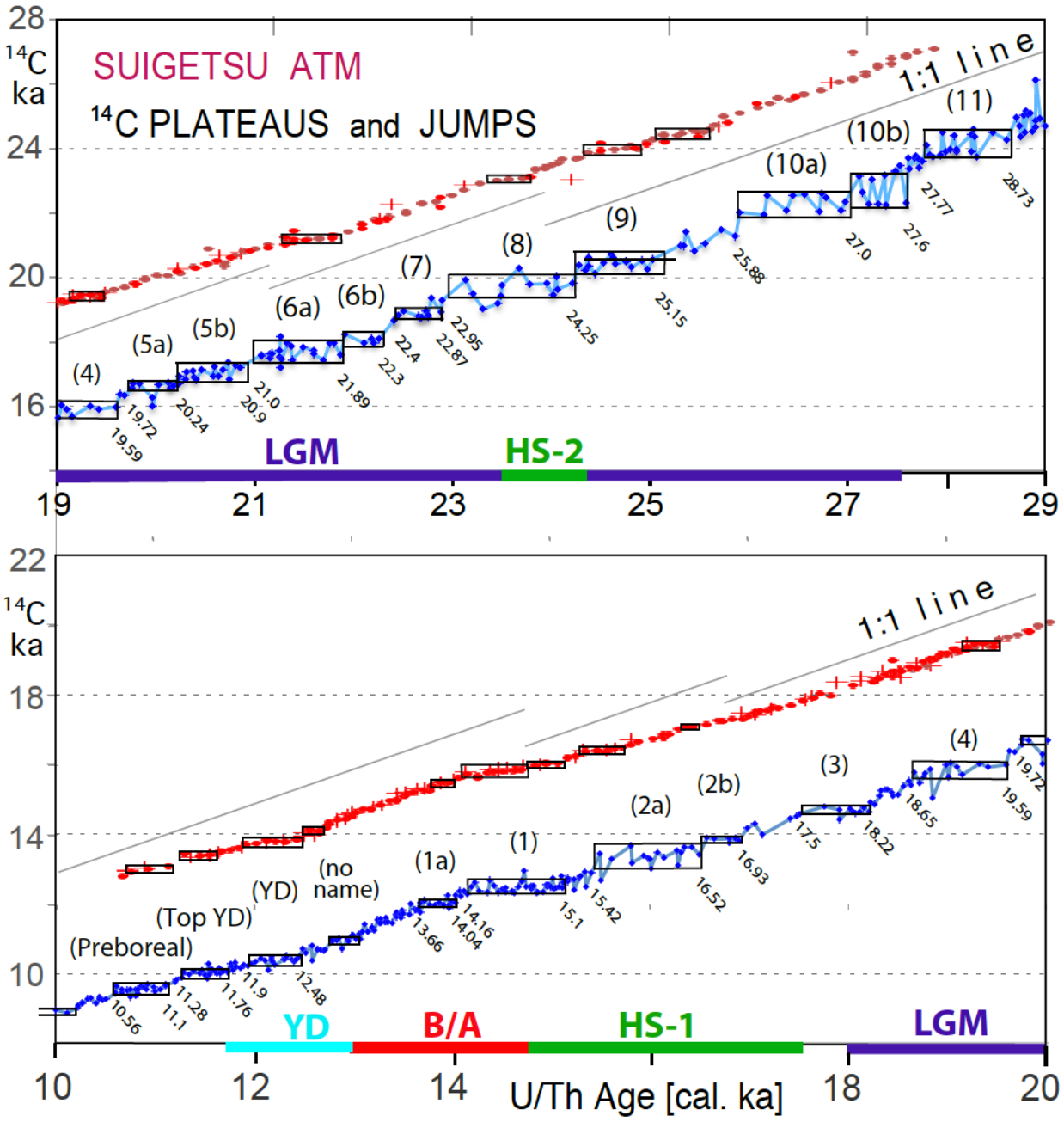

1319

1320

1321

~~V~~ Fig. 2. High-resolution record of atmospheric ^{14}C jumps and plateaus (= suite of labeled horizontal boxes that envelop scatter bands of largely constant ^{14}C ages extending over >300 cal. yr) in a sediment section of Lake Suigetsu vs. tree ring-based ^{14}C jumps and plateaus 10–14.5 cal. ka (Reimer et al., 2013). Blue line averages paired double and triple ^{14}C ages of Suigetsu plant macrofossils. Age control points (cal. ka) follow varve counts (Schlolaut et al., 2018) and U/Th model-based ages of Bronk Ramsey et al. (2012). YD = Younger Dryas, B/A = Bølling-Allerød.

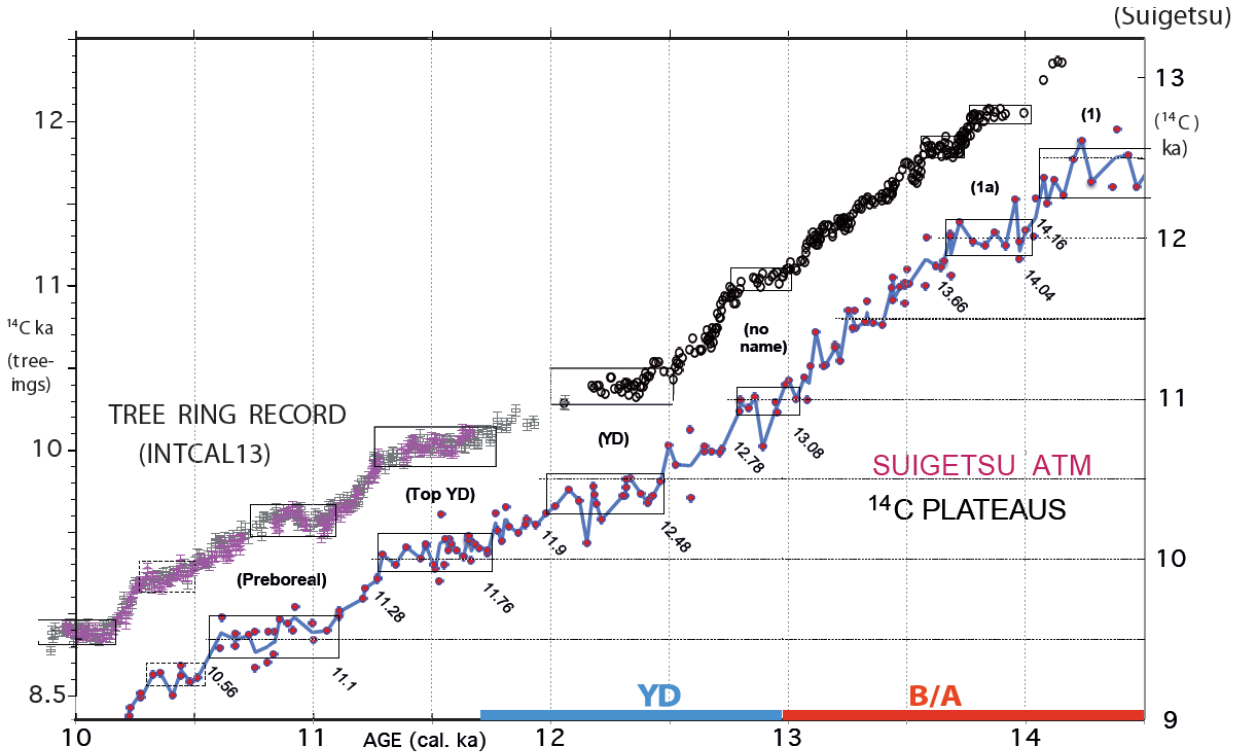

~~V~~ Fig. 3. Difference between Hulu Cave U/Th-based model ages (Southon et al., 2012; Bronk Ramsey et al., 2012; Cheng et al., 2018) and varve count-based cal. ages for atmospheric ^{14}C plateau boundaries in Lake Suigetsu sediment record (Schlolaut et al., 2018) (Sarnthein et al., 2015, suppl. and revised), displayed on the U/Th-based time scale 13–27 cal. ka.

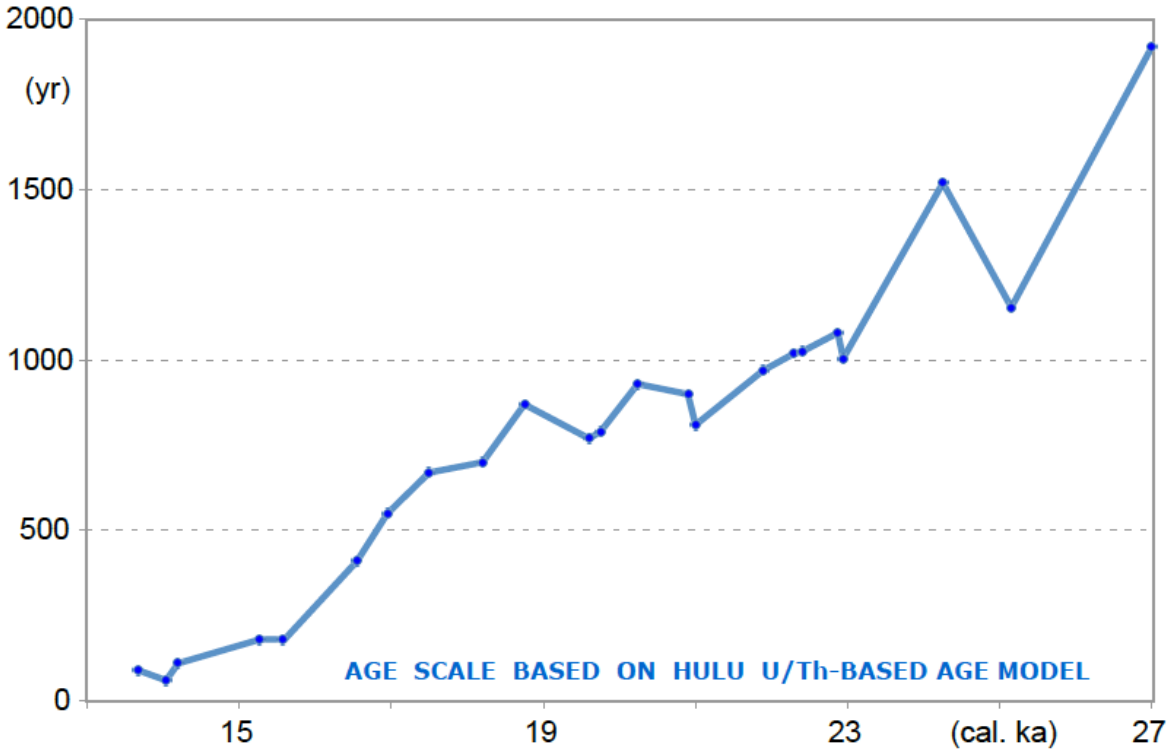

~~V~~ Fig. 4 a and b. Atmospheric ^{14}C ages and plateaus (horizontal boxes) deduced from ^{10}Be production rates vs. GICC05 age scale (Adolphi et al., 2018) compared to the Suigetsu record of atmospheric ^{14}C plateaus vs. Hulu U/Th-based model ages (Southon et al., 2012; Cheng et al., 2018) for the intervals a) 10-20 and b) 19-29 cal ka BP.

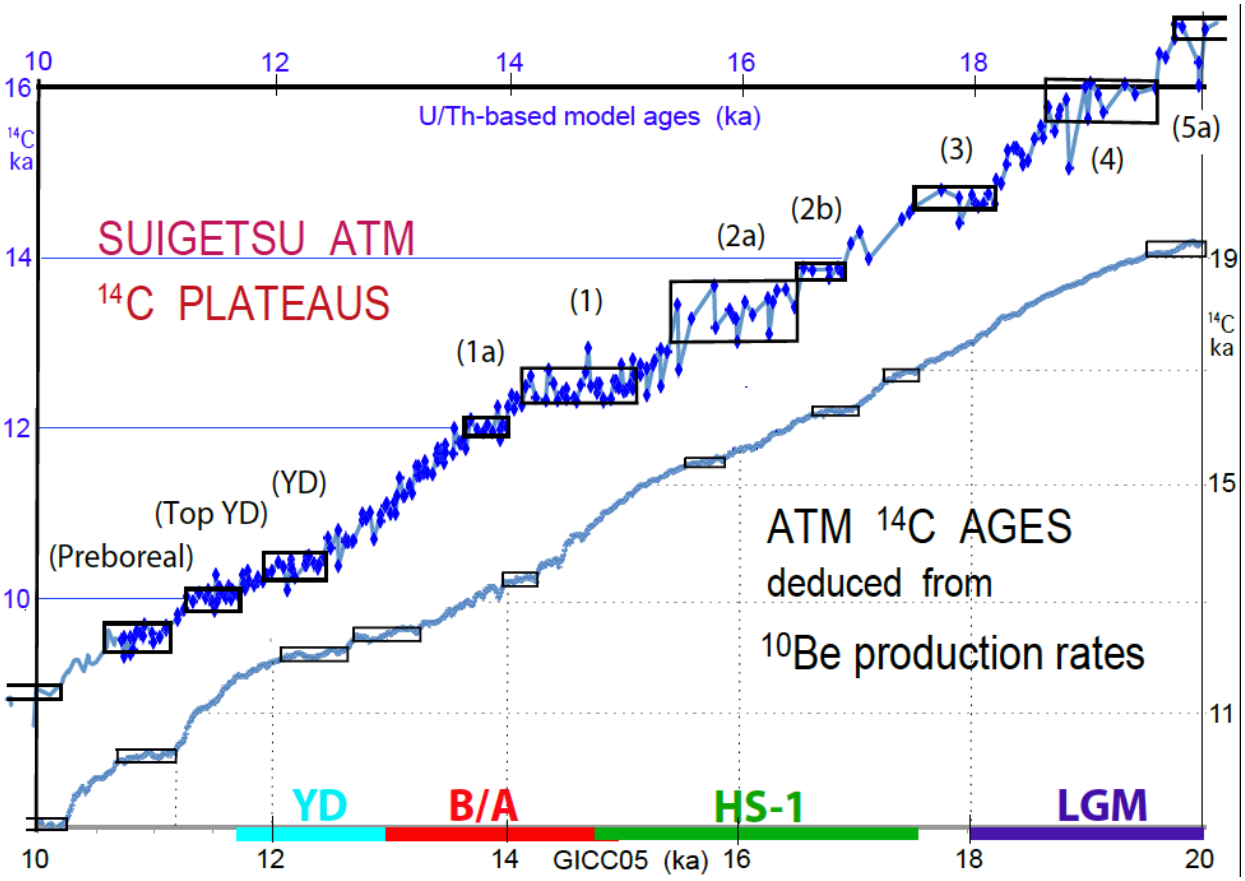

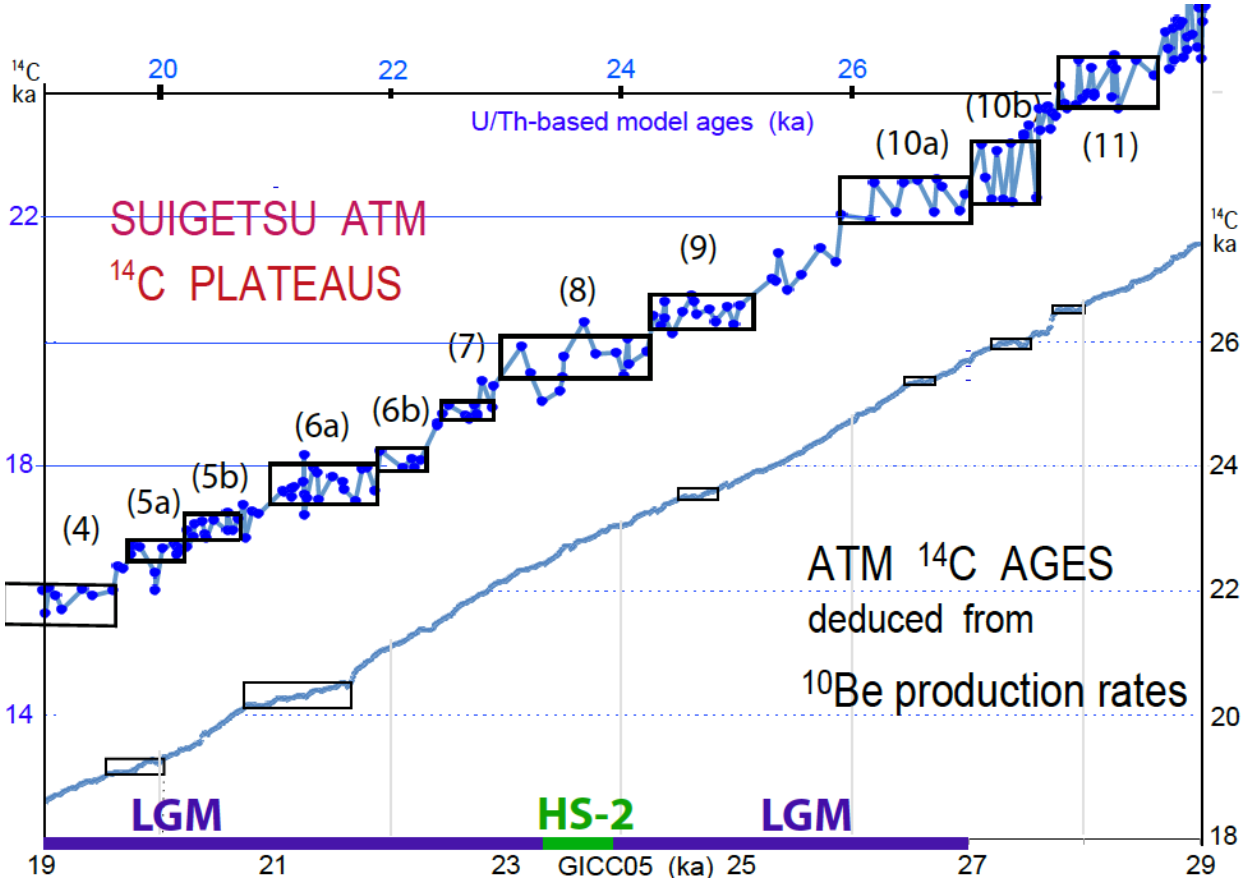
14C ka
20
22
24
26
U/Th-based model ages (ka)
SUIGETSU ATM
14C PLATEAUS
(4)
(5a)
(5b)
(6a)
(6b)
(7)
(8)
(9)
(10a)
(10b)
(11)
ATM 14C AGES
deduced from
10Be production rates
LGM
HS-2
LGM
GICC05 (ka)
19
21
23
25
27
29
18
20
22
24
26

~~V~~ Fig. 5. Sediment facies and microfacies zones in Lake Suigetsu Core SG06, ~13–32 m depth (simplified and suppl. from Schlolaut et al., 2018). Microscopy-based frequency of siderite layers with quality level 1–3 (= running average of layer counts per 20 cm thick sediment section) serves as measure of seasonal lamination quality and shows gradual transitions between varved and poorly varved sediment sections. Rounded varve ages are microscopy based and constrain age of major facies and microfacies boundaries. ANI I to ANI III mark core sections with ultrafine lamination due to sedimentation rate minima, AT marks tephra layer named AT, 'Event layers' label major thin mud slides probably earth quake-induced.s

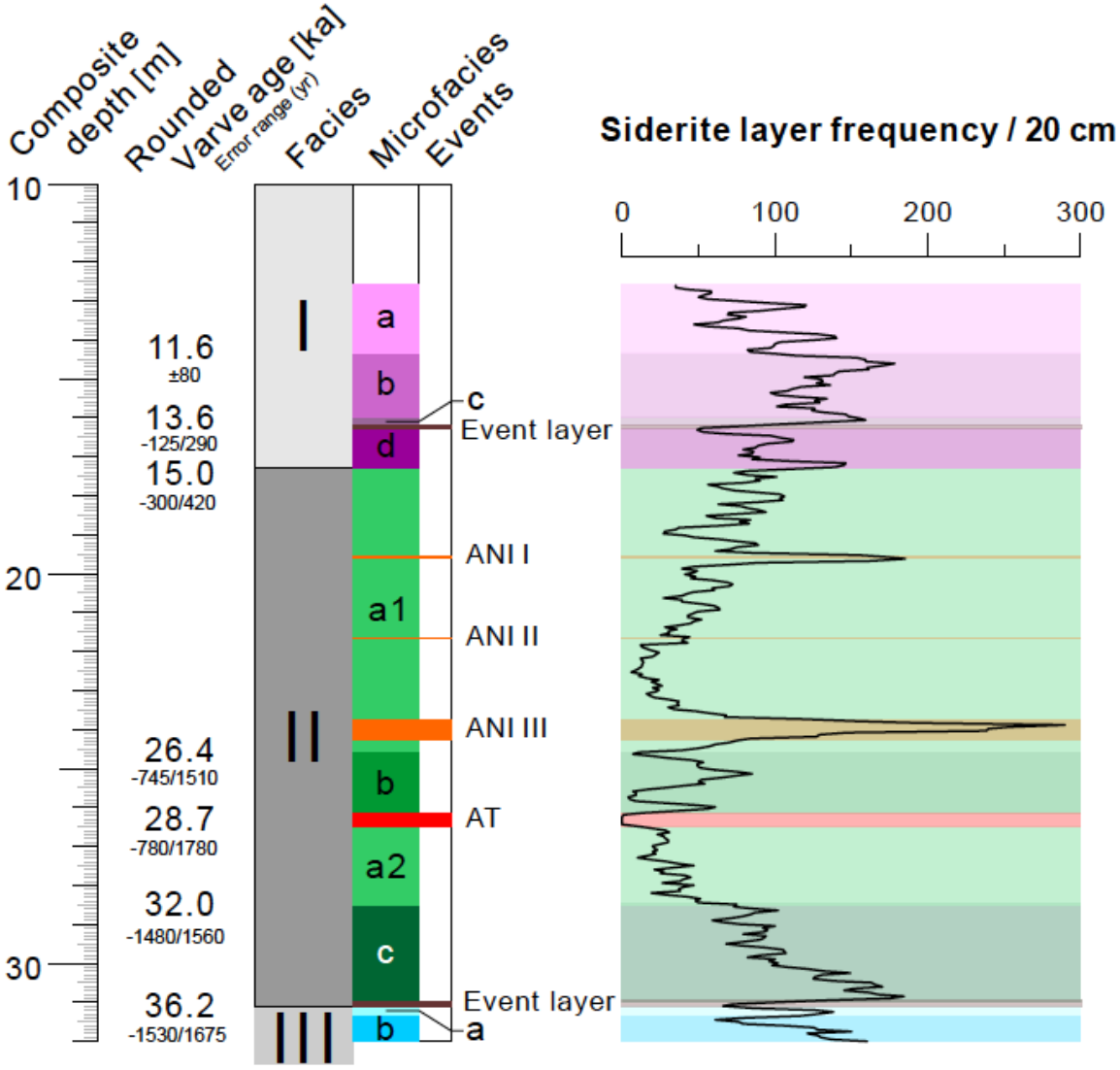

~~V~~ Fig. 6 (a). Four sudden steps (pink bars) in the deglacial atmospheric CO_2 rise at West Antarctic Ice Sheet Divide ice core (WDC) reflect events of fast ocean degassing, that may have contributed to the origin of deglacial ^{14}C plateaus. Age control based on ice cores (Marcott et al., 2014). (b) The steps are compared to suite of atmospheric ^{14}C plateaus dated by Hulu U/Th-based model ages (Bronk Ramsey et al., 2012). Hol = Holocene; YD = Younger Dryas; B/A = Bølling-Allerød; HS = Heinrich stadials 1 and 2; LGM = Last Glacial Maximum, GIS-2 = Greenland interstadial 2.

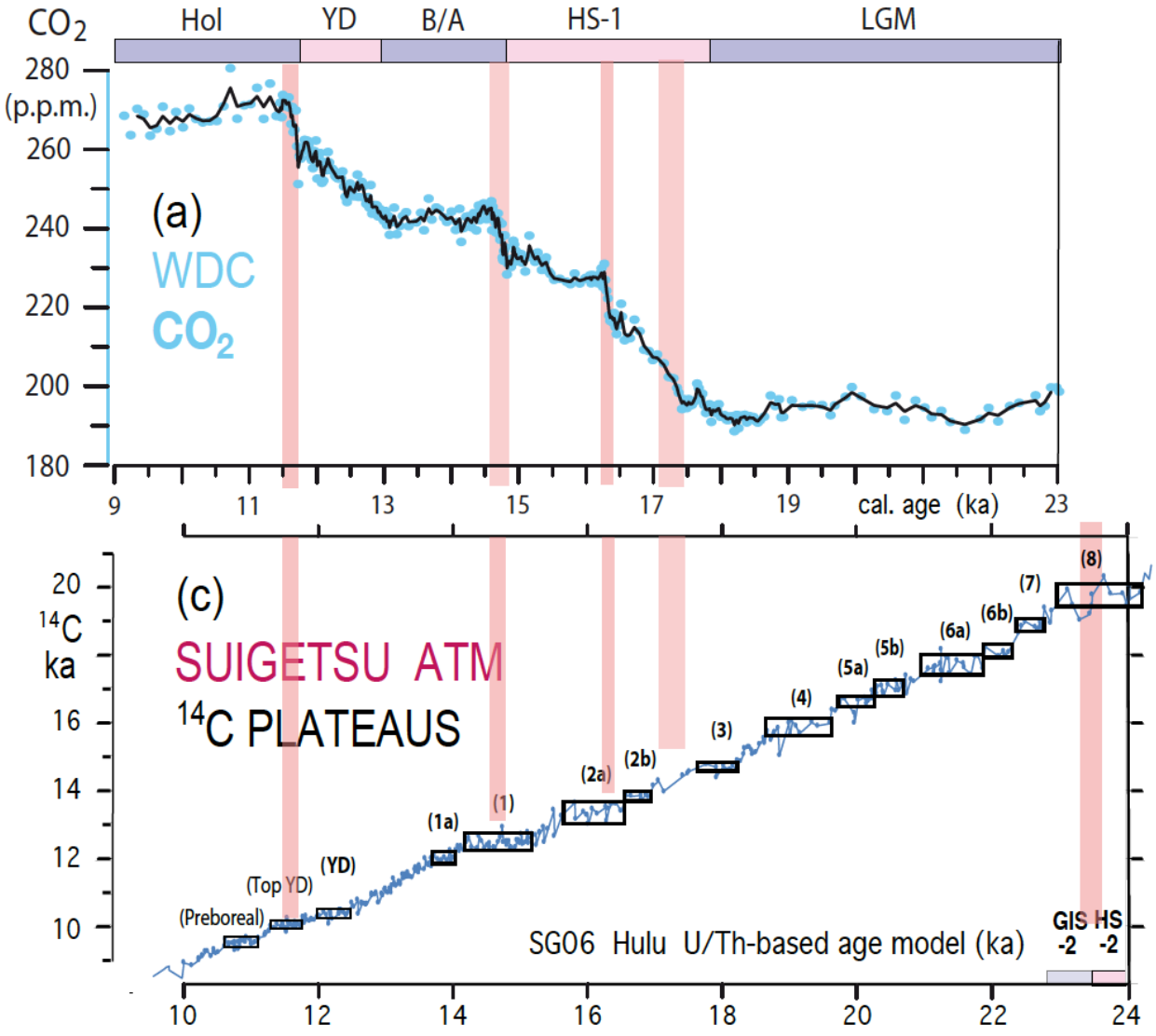

1395 ~~V~~ Fig. 7. Location (a) and water depth (km) (b) of sediment cores with age control based

1396 on ^{14}C plateau tuning. ^{14}C reservoir ages of cores labeled with 'w' are derived from

1397 samples with paired wood chunks and planktic foraminifers.

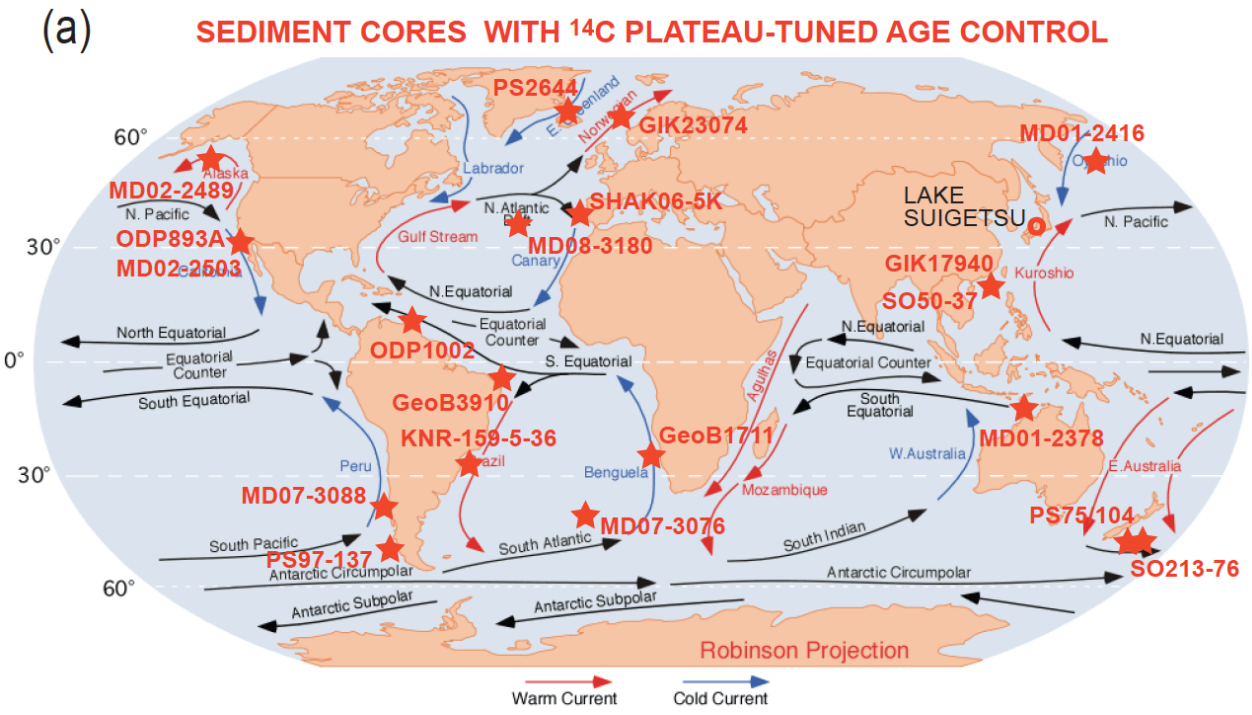

1398

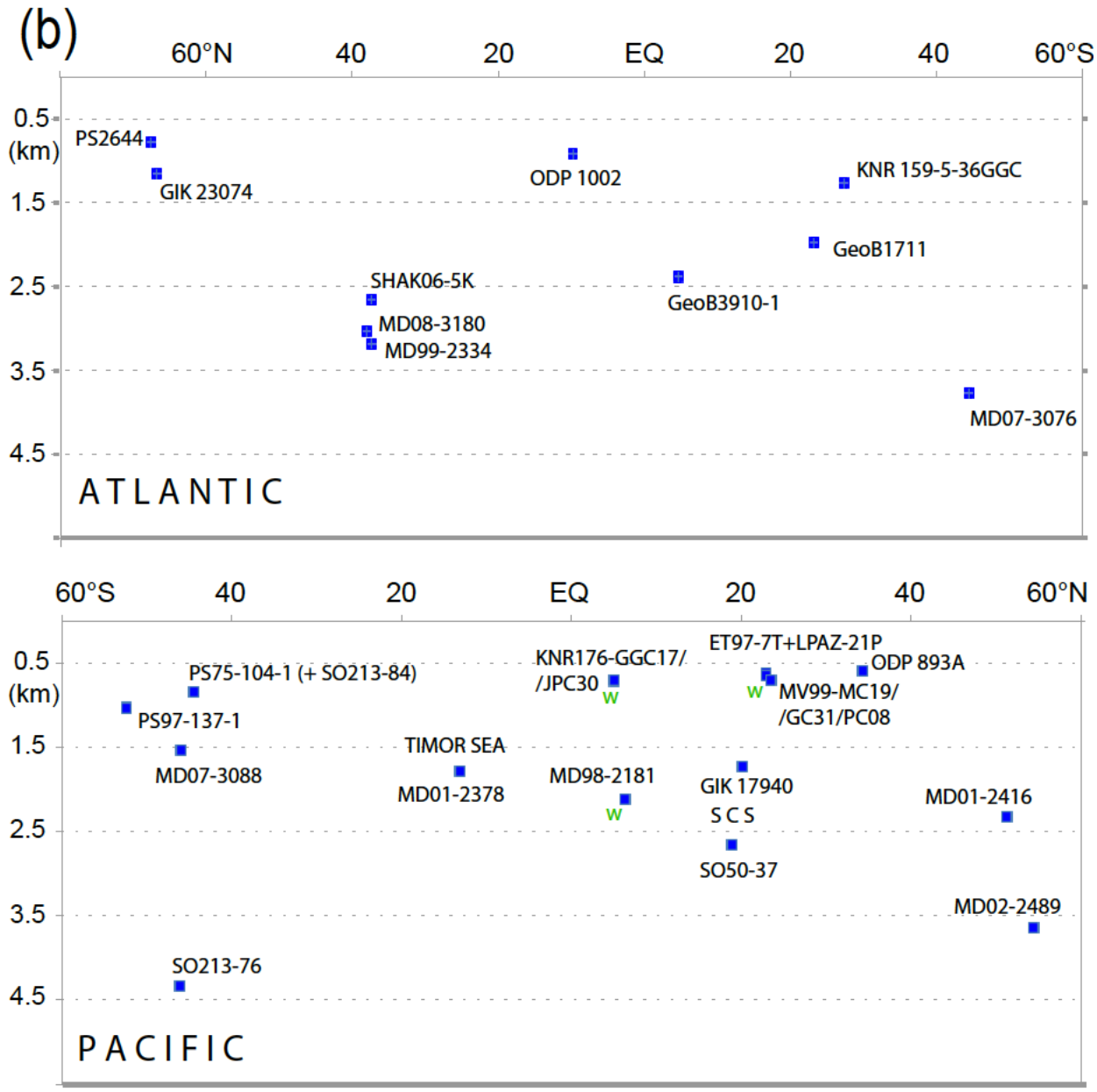

1399

1400

1401 ~~V~~ Fig. 8. Global distribution of ^{14}C reservoir ages of Late LGM surface waters estimated
1402 (a) by means of ^{14}C plateau tuning of planktic 14C records. (b) Model-based estimates
1403 (GCM of Muglia et al., 2018, assuming an AMOC strength of 13 Sv) for sites with
1404 planktic foraminifera-based age values. X-Y graph (c) and map (d) show (rounded)
1405 differences between observed and modeled values and their intra-LGM trends. Minor
1406 differences are displayed in magenta, larger differences of >400 yr in red. Planktic
1407 habitat depths and model estimates are largely confined to 0–100 m water depth.

Arrows of surface currents delineate different sea regions important to assess potential limits of spatial extrapolation of reservoir ages. Distribution of core numbers and references for ^{14}C records are given in Table 3a-c and Fig. 7a.

Fig. 8a

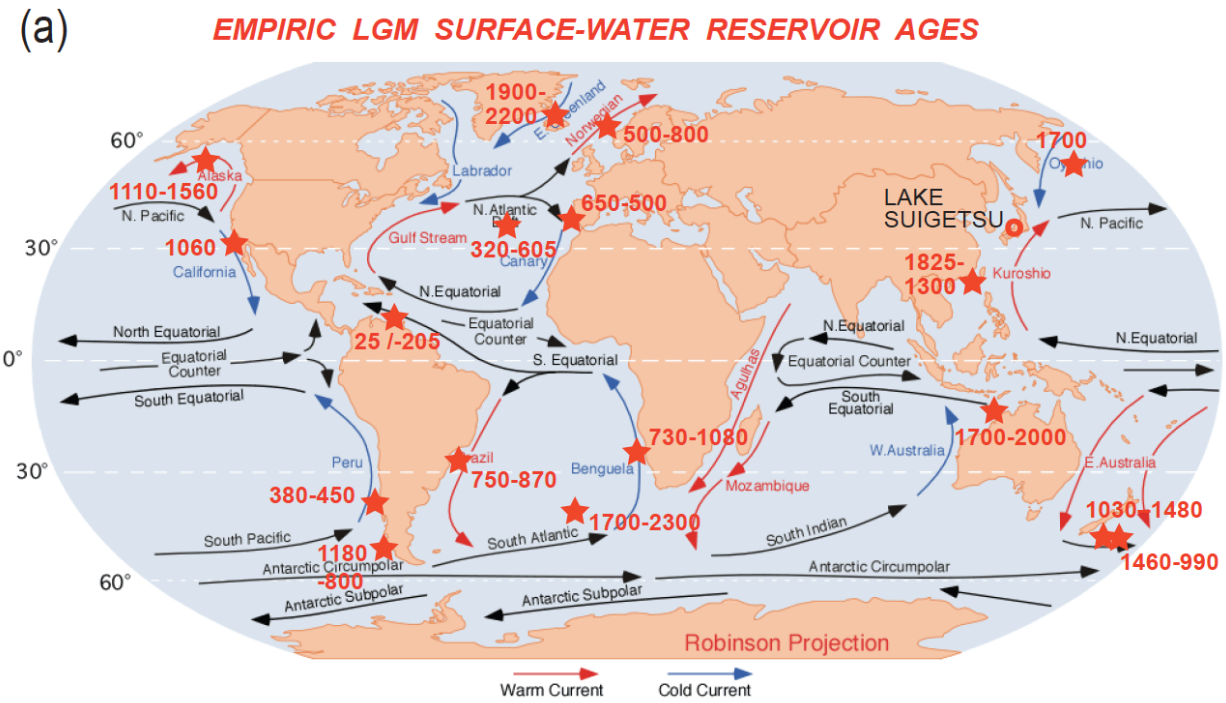

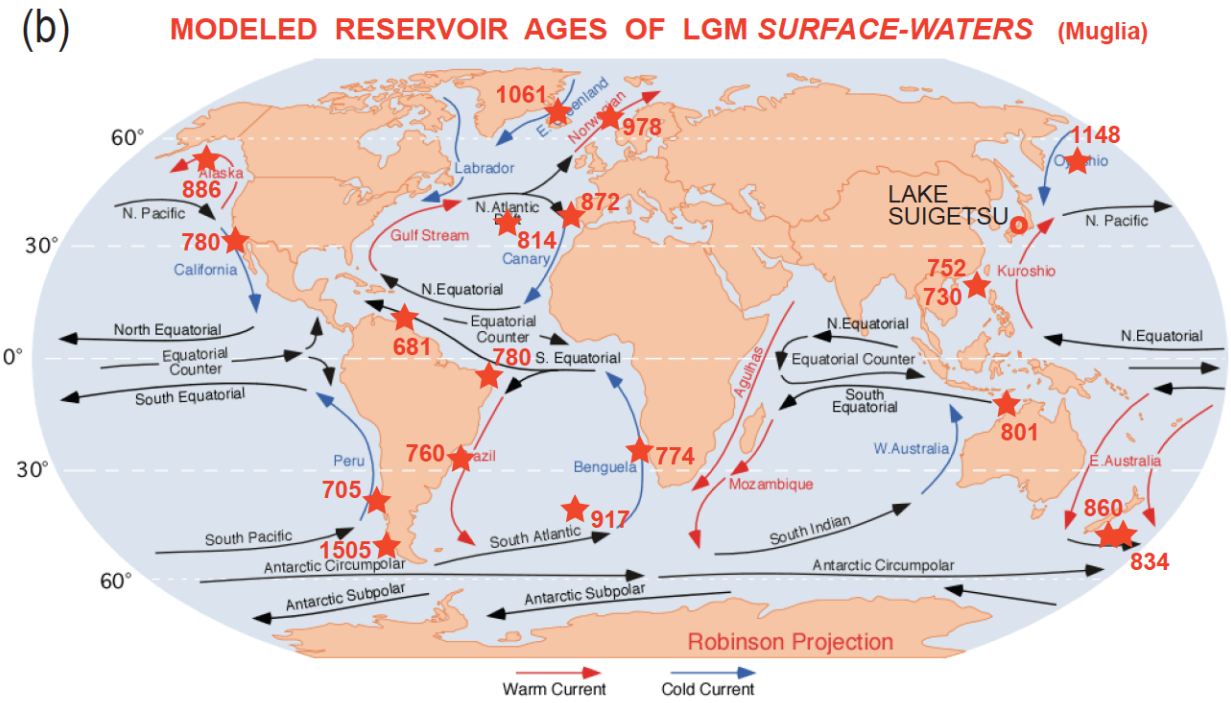

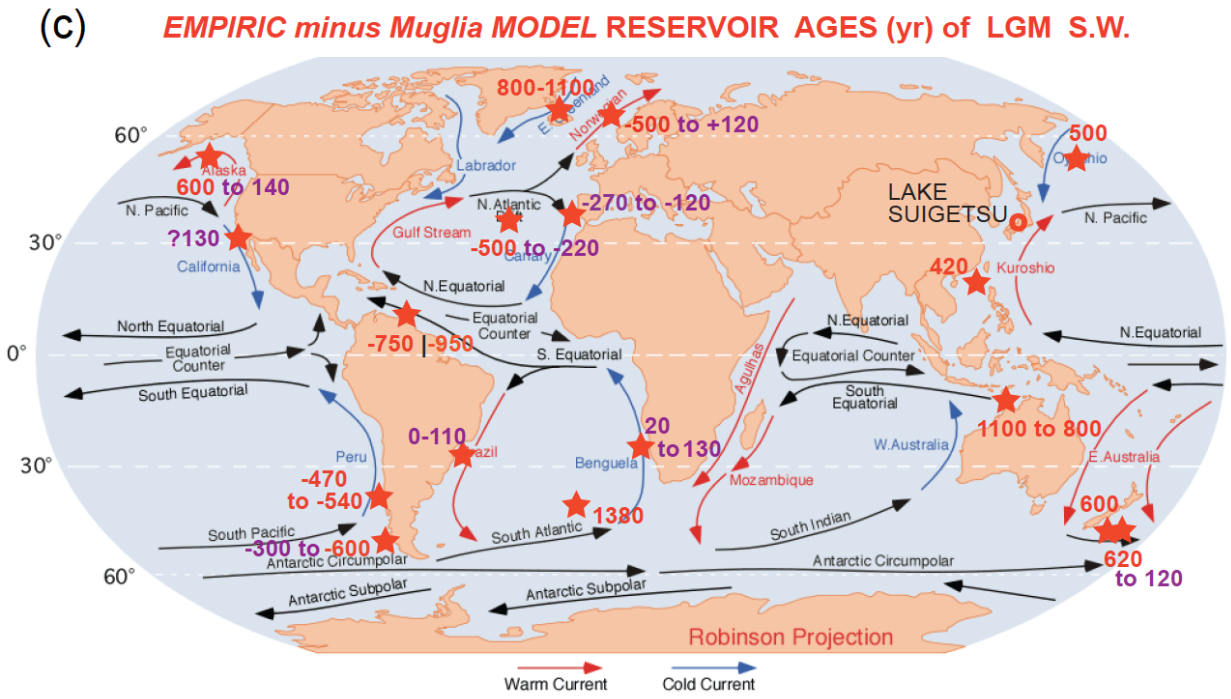

1413

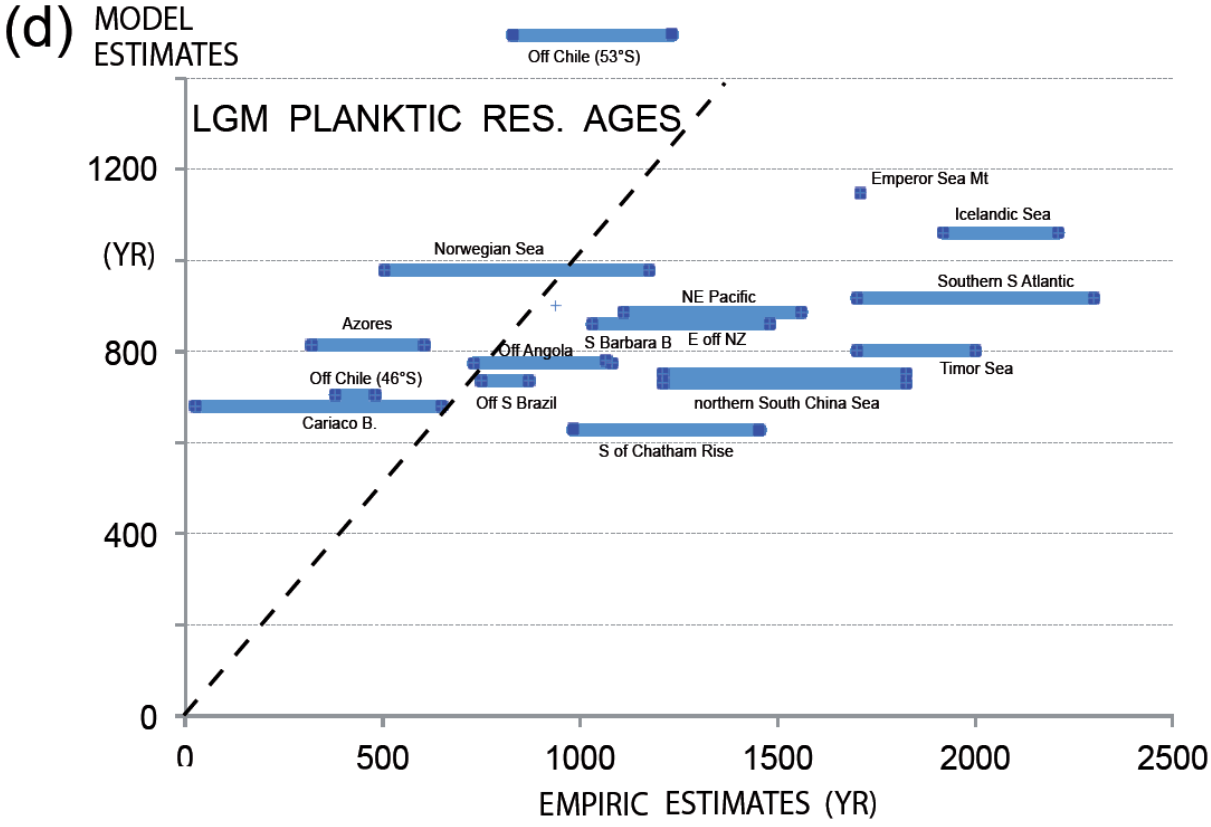

1414

1415

1416 ~~V~~ Fig. 9. SW–NE transect of ^{14}C reservoir age and changes in ventilation age across

1417 sites GIK17940 and SO50-37 in the South China Sea during late LGM (^{14}C Plateaus 5

and 4; upper panel) and HS-1 (lower panel). Insert map shows location of transect and core locations. Core locations are given in Fig. 7. An extreme epibenthic $\delta^{13}C$ minimum in far southwest (Core GIK17964; Sarnthein et al., 1999) reflects an LGM incursion of Lower/Upper Pacific Deep Waters (L./ U. PAC DW) with extremely high ^{14}C ventilation age and DIC enrichment in contrast to a low ventilation age of North Pacific Deep Water (N. PAC DW). Arrows show direction of potential deep and intermediate-water currents.

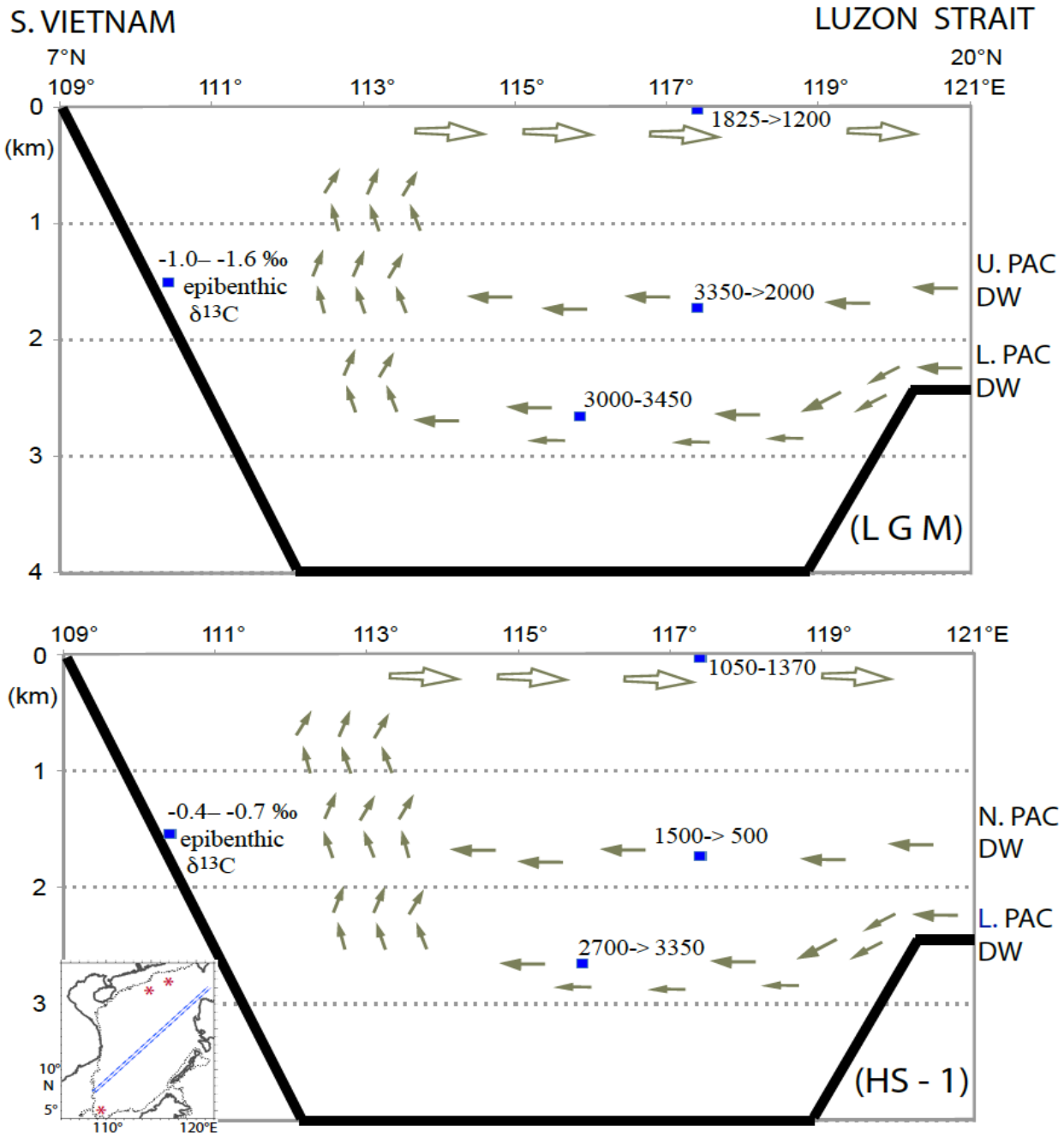

~~V~~ Fig. 10. 2D transects of the geometries of global ocean MOC. Arrows (blue = high, yellow = poor ventilation) suggest average deep and intermediate-water currents that follow the gradient from low to high benthic ventilation ages based on paired planktic ^{14}C reservoir ages derived by means of ^{14}C plateau tuning technique (Sarnthein et al., 2013, Balmer et al., 2018, Küssner et al., 2020 subm.). At some Pacific sites reservoir ages are based on paired ^{14}C ages of planktic foraminifera and wood chunks (marked by green 'w'; Sarnthein et al., 2015; Zhao and Keigwin, 2018, Rafter et al., 2018). Red arrows suggest poleward warm surface water currents. Zigzag lines indicate major frontal systems separating counter rotating ocean currents (e.g., W of Portugal and N of MD07-307; after Skinner et al., 2014). (a) Late LGM circulation geometry (21–18.7 cal. ka), largely similar to today. Note the major east-west gradient of ventilation ages in the central North Atlantic, between Portugal (PORT) and Mid-Atlantic Ridge W of Azores (MAR). (b) HS-1 benthic ventilation ages reveal a short-lasting MOC reversal leading to Atlantic-style overturning in the subpolar North Pacific and coeval Pacific-style stratification in the northern North Atlantic, with seesaw-style reversals of global MOC at the onset and end of early HS-1 (first proposed by Broecker et al., 1985, however, for LGM times). Increased ventilation ages reflect enhanced uptake of dissolved carbon in the LGM deep ocean (Sarnthein et al., 2013), major drops suggest major degassing of CO_2 from both the deep Southern Ocean and North Pacific during early HS-1. – SCS = South China Sea. AABW = Antarctic Bottom Water; AAIW = Antarctic Intermediate Water. NADW = North Atlantic Deep Water. Small arrows within age numbers reflect temporal trends. Many arrows are speculative using circumstantial evidence of benthic $\delta^{13}C$ records and local Coriolis forcing at high-latitude sites per analogy to modern scenarios. Location of sediment cores are given in Fig. 7, short-term variations in planktic and benthic ^{14}C reservoir/ventilation age in Suppl. Fig. S2 and Table 3.

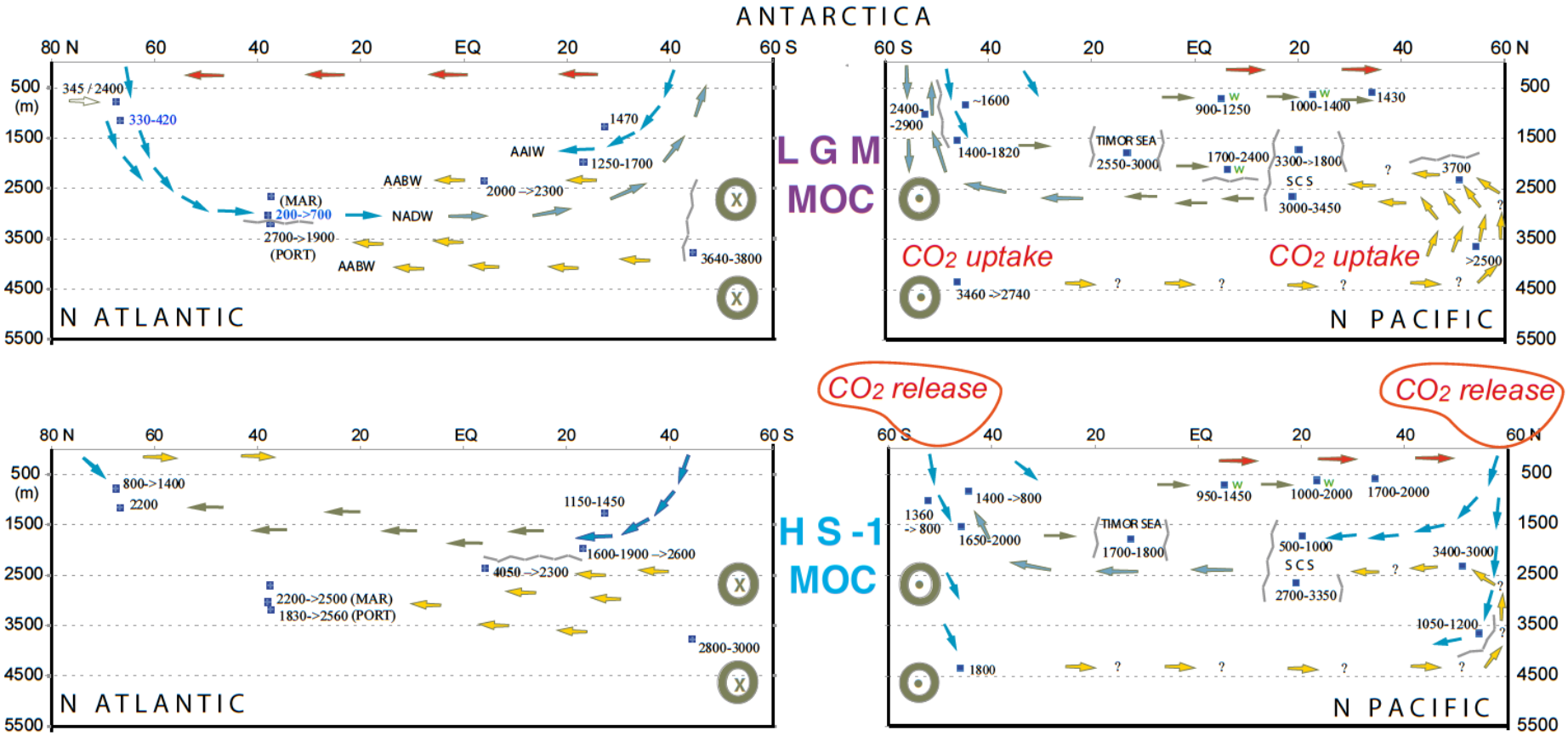
ANTARCTICA
80 N
60
40
20
EQ
20
40
60 S
500
(m)
1500
2500
3500
4500
5500
345 / 2400
330-420
1470
AAIW
1250-1700
AABW
2000 ->2300
(MAR)
200->700
NADW
2700->1900
(PORT)
AABW
3640-3800
N ATLANTIC
L G M
MOC
60 S
60 N
2400
-2900
~1600
1400-1820
TIMOR SEA
2550-3000
900-1250
1000-1400
1430
1700-2400
3300->1800
SCS
3000-3450
3700
>2500
CO2 uptake
CO2 uptake
3460 ->2740
N PACIFIC
CO2 release
CO2 release
800->1400
2200
1150-1450
1600-1900 ->2600
4050 ->2300
2200->2500 (MAR)
1830->2560 (PORT)
2800-3000
N ATLANTIC
H S -1
MOC
1400 ->800
1360
-> 800
1650-2000
TIMOR SEA
1700-1800
950-1450
1000-2000
1700-2000
500-1000
SCS
2700-3350
3400-3000
1050-1200
1800
N PACIFIC

1451

1452 ~~V~~ Fig. 11. Global distribution of ^{14}C reservoir ages obtained (a) for late LGM

1453 intermediate waters (100–1800 m w.d.) and (b) for LGM deep waters (>1800 m w.d.,

1454 including Site GIK 23074 at 1157 m in the Norwegian Sea).

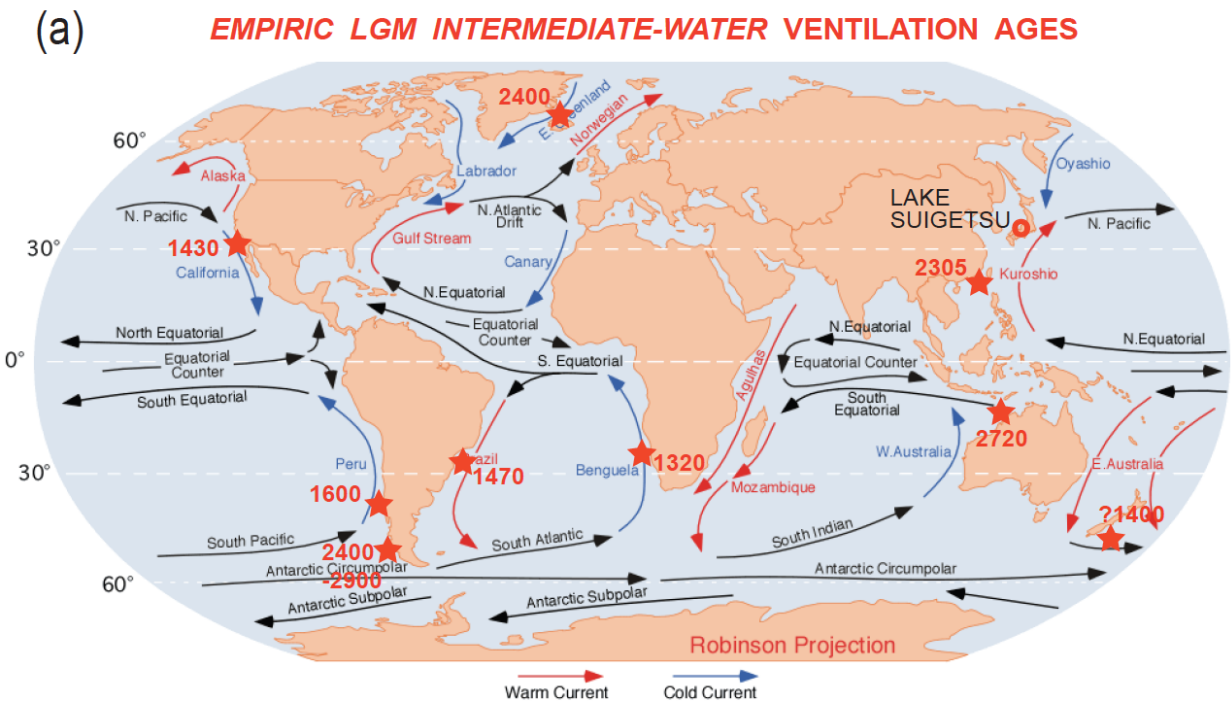

1455

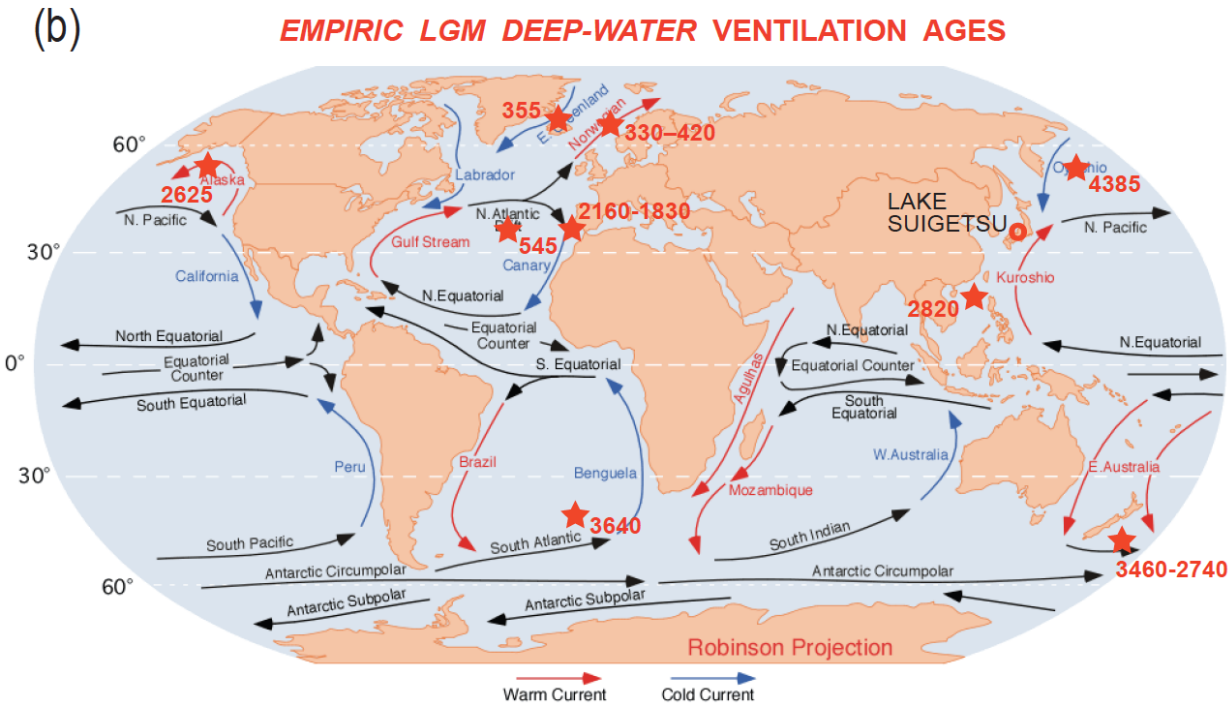

1456